FLINDERS UNIVERSITY OF SOUTH AUSTRALIA

THE ROLE OF SIRTUIN 1 DURING HIGH-FAT FEEDING

KAMELYA ALIAKBARI

Master of Biotechnology Studies

Faculty of Health Sciences

Supervisor: Dr Elke Sokoya

Department of Human Physiology

Co-supervisor: Dr Karen Lower

Department of Haematology

This thesis is submitted in partial fulfilment of the requirements of the Master of Biotechnology degree at Flinders University of South Australia. December 2014

TABLE OF CONTENTS

DECLARATION

I hereby certify that this thesis entitles "The Role of Sirtuin 1 During High-Fat Feeding" does not contain material which has been accepted for the award of any degree or diploma; and to the best of my knowledge and belief it does not contain any material previously published or written by another person except where due reference is made in the text of this thesis.

Kamelya Aliakbari

December 5th, 2014

ACKNOWLEDGEMENTS

LIST OF ABBREVIATIONS

Abbreviation	Definition
ADP	Adenosine diphosphate ribose
Akt	Protein kinase B
BAC	Bacterial artificial chromosome
BAX	Apoptosis regulator gene
BMI	Body mass index
bp	Base pair
cDNA	Complementary DNA
cGMP	Cyclic guanosine monophosphate
Ct	Cycle threshold
DEPC	Diethylpyrocarbonate
DNA	Deoxyribonucleic acid
DNase	Deoxyribonuclease
DTT	Dithiothreitol
Duox1	Dual oxidase 1
Duox2	Dual oxidase 2
E	Efficiency
eNOS	Endothelial nitric oxide synthase
FOXO	Forkhead box O3
GADD45	Growth arrest and DNA-damage-inducible protein
GOI	Gene of interest
HDL	High density lipoprotein
HFD	High fat diet
H_2O_2	Hydrogen peroxide
IDT	Integrated DNA Technology
iNOS	Inducible nitric oxide synthase
kDa	The unified atomic mass unit
MnSOD	Extracellular superoxide dismutase
NAD^+	Nicotinamide adenine dinucleotide (Oxidised)
NADH	Nicotinamide adenine dinucleotide (Reduced)
NADPH	Nicotinamide adenine dinucleotide phosphate
NC	Normal chow
NCF1	Neutrophil cytosol factor 1
NO	Nitric oxide
NOSs	Nitric oxide synthase family of enzymes
Nox1	NADPH oxidase 1
Nox2	NADPH oxidase 2
Nox3	NADPH oxidase 3
Nox4	NADPH oxidase 4
Nox5	NADPH oxidase 5

O_2	Molecular oxygen
$O_2\bullet^-$	Superoxide
$OH\bullet$	Hydroxyl radicals
$ONOO^-$	Proxynitrate
PAGE	Polyacrylamide gel electrophoresis
PARP-1	Poly adenosine diphosphate ribose polymerase 1
PBS	Phosphate buffered saline
PCNA	Proliferating cell nuclear antigen
PGC-1α	Peroxisome proliferator-activated receptor gamma coactivator 1-alpha
PPARα	Peroxisome proliferator-activated receptor alpha
PPAR-γ	Peroxisome proliferator-activated receptor gamma
PUMA	p53 upregulated modulator of apoptosis
PVDF	Polyvinylidene fluoride
p21	Cyclin-dependent kinase inhibitor 1
p53	Tumor suppressor p53
REF	Reference gene
RIN	RNA integrity number
RNA	Ribonucleic acid
RNS	Reactive nitrogen species
ROS	Reactive oxygen species
SDS	Sodium dodecyl sulfate
SEM	Standard standard error of the mean
SREBP1	Sterol regulatory element-binding transcription factor 1
SIRT1	Sirtuin 1
SIRT1-KI	Sirtuin 1 knockin mice
SOD	Superoxide dismutase
SOD1	Cytosolic superoxide dismutase
SOD2	Extracellular superoxide dismutase
SOD3	Mitochondrial superoxide dismutase
TBE	Tris-borate-EDTA
TNF-α	Tumor necrosis factor alpha
UCP2	Uncoupling protein 2
WAT	White adipose tissue
WHO	World Health Organisation
WT	Wildtype

1. ABSTRACT

Background: More than half of the Australian adult population is overweight or obese. High-fat feeding is the main culprit for these staggering statistics. Oxidative stress, inflammation and decreased nitric oxide bioavailability in obese patients increase their likelihood of developing stroke or dementia.

Purpose: Sirtuin 1 (SIRT1) is a protein deacetylase with known antioxidant properties and ability to enhance nitric oxide bioavailability. Studies from our laboratory and others have shown that high-fat feeding leads to SIRT1 depletion within the vasculature. In the present study, we tested the hypothesis that SIRT1 overexpression during high-fat feeding would attenuate the phenotypes of vascular ageing, including inflammation and oxidative stress.

Methods: Wildtype (WT) and SIRT1 overexpressing mice (SIRT1-KI) were fed either a normal diet or high-fat diet for two months. At the end of the study, whole blood, plasma and vascular samples were obtained and stored for analysis.

Results: WT mice on a high-fat diet displayed decreased SIRT1 protein expression and increased nitrotyrosine expression, as measured in the carotid artery, which were both prevented in SIRT1-KI mice.

Conclusions: Our results highlight the potential benefits of targeting SIRT1 as a therapeutic strategy in reducing the clinical complications associated with vascular impairment during high-fat feeding.

2. INTRODUCTION

2.1 Obesity

Obesity has become a major public health concern in Australia with more than 50 per cent of adults being classified as overweight or obese (Statistics, 2012).Obesity increases the risk of cardiovascular disease, stroke and dementia, thereby reducing life expectancy. Consequently, obesity reduces quality of life and places a significant burden on the Australian Health Care system.

Obesity is a chronic disease that arises from a combination of variables including, sedentary lifestyle, psychological, and metabolic disorders (Healy et al., 2008, Manson et al., 2004). It is defined as an increase in the percentage of body fat compared to total body weight (Bray and York, 1971). The World Health Organization (WHO) defines obesity as a body-mass index (BMI) of greater than 30 kg/m^2 which distinguishes it from being overweight (BMI $\geq$ 25 kg/m^2)(WHO, 2000).

Obesity is caused by an imbalance between energy intake and expenditure. Excess energy intake can result in an increase in adipose tissue (fat) (Hotamisligil, 2006). Obesity has significant implications on health but it can become even more complicated with a number of comorbid conditions, such as Alzheimer's disease, type II diabetes, stroke and cancer (Codoner-Franch et al., 2011, Eyre et al., 2004).

Animal models, such as rodents fed with a high fat diet, allow us to study the mechanisms underscoring obesity, in the hope of finding new therapeutic targets that could be used to deter the onset of diabetes-related vascular disease (Buettner et al., 2007).

2.1.1   Statistics of Obesity

Results from the 2011–12 Australian-wide survey showed that almost two thirds of the adult population was overweight; half of these were obese (Statistics, 2012). A diet high in saturated fat increases the risk of heart disease and stroke. It is estimated that obesity is the cause of one in every three cases of coronary heart disease and one in every ten cases of stroke worldwide (World Heart Federation, 2014).

In the last 20 years, the prevalence of obesity in Australia has more than doubled. Health problems related to excess body weight not only impact individuals but also their families. Moreover, the effect of obesity on health, places a huge economic burden on the healthcare system and therefore the society (Wang et al., 2008).

2.2   Oxidative Stress

2.2.1   Excessive Reactive Oxygen Species Cause Oxidative Stress

Reactive oxygen species (ROS) are molecules that contain O_2 and are very unstable. Superoxide ($O_2^{\bullet-}$), hydrogen peroxide (H_2O_2), and hydroxyl radicals ($OH^{\bullet}$) are examples of ROS. Some of them are free radicals that contain an unpaired electron, making them extremely reactive. Under normal conditions, the amount of ROS that is produced in the body is counterbalanced by endogenous antioxidants that help to scavenge free radicals. Indeed, low concentrations of ROS are necessary for normal cell redox status, intracellular signaling and cell function (Trachootham et al., 2008). However in disease, ROS production can exceed the capability of the antioxidant defence mechanisms, leading to excessive ROS levels. This condition is known as oxidative stress. Sustained high levels of ROS are destructive by damaging proteins, carbohydrates, lipids and DNA (Dahiya et al., 2013, Schrauwen et al., 2006a).

2.2.2 Antioxidant Enzymes

The key antioxidant enzymes are superoxide dismutase (SOD), glutathione peroxidase and catalase. The role of SOD is to convert superoxide into H_2O_2. There are three isoforms of SOD, cytosolic (SOD1), extracellular (SOD3) and mitochondrial (MnSOD or SOD2). Glutathione peroxidase and catalase reduce H_2O_2 into stable O_2.

2.2.3 Where Does Superoxide Come From?

One of the most important ROS is superoxide (see **Figure 2.1**). A dominant source of superoxide is the mitochondria, as a by-product of oxidative phosphorylation. Excessive superoxide production from the mitochondria can lead to mitochondrial dysfunction and ensuing apoptosis and necrosis (Jaeschke et al., 2002). In obesity, free fatty acids circulating in the blood promotes mitochondrial uncoupling (Schrauwen et al., 2006a, Schrauwen et al., 2006b, Weigle et al., 1998) that may lead to insulin resistance by activation of TNF-α (Chen et al., 2010). TNF-α activates NADPH oxidase in vascular smooth muscle cells and increases the production of ROS by decreasing NO bioavailability (see *NO Bioavailability*) (Evans et al., 2002).

Another source of superoxide is via the enzymatic activity of xanthine oxidase. Xanthine oxidase metabolises hypoxanthine and xanthine to form ROS ($O_2\bullet^-$ and H_2O_2). By using NAD^+ as cofactor, xanthine oxidase produces H_2O_2 and NADH thereby enhancing mitochondrial electron transport chain activity and increasing ROS production (Ichida et al., 2012).
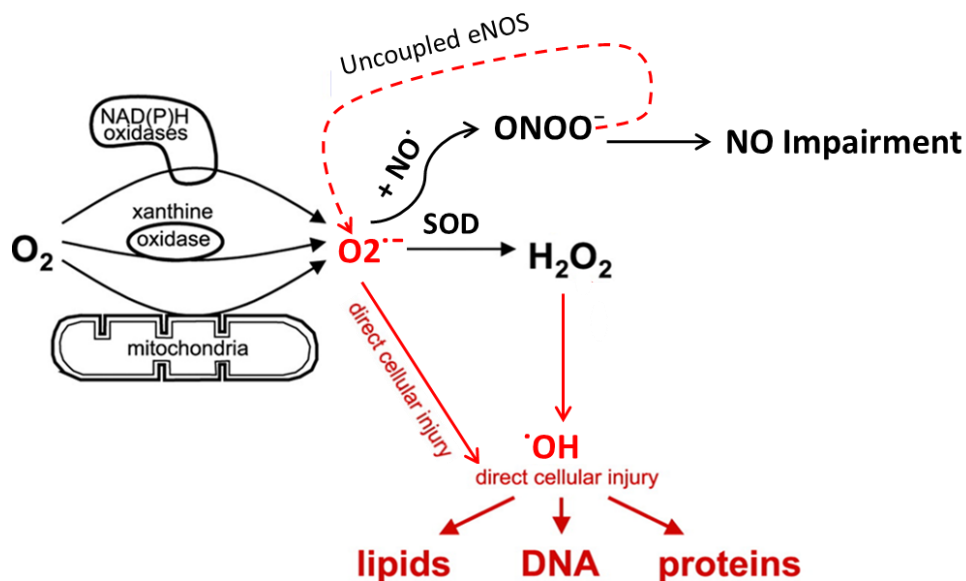
Figure 2.1.   Reactive oxygen metabolism. Superoxide can be produced by mitochondria, xanthine oxidase or NADPH oxidase. It can cause molecular damage, directly or by interacting with NO and resulting in eNOS uncoupling (Becker, 2004).

Superoxide is also formed from the enzyme NADPH oxidase, a complex consisting of the cytosolic p47phox and p67phox subunits, the membrane-bound Nox and p22phox subunits, and a small G protein Rac (Hori et al., 2013). Seven Nox isoforms have been found in mammalian cells: namely Nox1, Nox2, Nox3, Nox4, Nox5 and Duox1 and 2. NADPH oxidase was first discovered in immune cells. Following stimulation, immune cells need to quickly synthesize microbicidal agents. To this end, the cells start by using NADPH oxidase to reduce molecular oxygen (O_2) to form superoxide, a process known as the "respiratory burst" (Segal and Jones, 1978) (Babior et al., 1973).

Recent studies have shown that NADPH oxidase (Nox1, Nox2, Nox4, and Nox5) is also expressed within the endothelial and smooth muscle cells of the vasculature

(Lassegue and Griendling, 2010). Vascular NADPH oxidases are one of the major sources of ROS in the cardiovascular system (Wu and Ballantyne, 2014, Lassegue and Griendling, 2010).

In obesity, the elevated numbers of white cells (Hardy et al., 2008) contribute to the increased production of superoxide as well as other ROS. Increased expression of Nox2 and Nox4 within the vasculature has also been shown (Lynch et al., 1997, Jiang et al., 2012).

A final source of superoxide is from the uncoupling of endothelial nitric oxide synthase (eNOS) (see *NO Bioavailability*). This results in the formation of superoxide rather than nitric oxide (NO).

2.2.4   Consequences of Superoxide Production

Superoxide is a highly reactive molecule that can react with NO to form peroxynitrite (ONOO$^-$). ONOO$^-$ belongs to the family of reactive nitrogen species (RNS), and is chemically unstable. It promotes nitration of tyrosine residues in proteins, leading to nitrotyrosine-containing proteins. Nitrotyrosine formation is often associated with inflammation (Hardy et al., 2008).

ONOO$^-$ can also inhibit manganese superoxide dismutase (MnSOD) activity, activate the nuclear enzyme poly (ADP-ribose) polymerase (PARP-1) and increase inducible (Kawashima and Yokoyama) expression, leading to further cellular dysfunction. Inducible NOS (Kawashima and Yokoyama, 2004b) belongs to the family of nitric

oxide synthase enzymes, involved in catalysing the production of nitric oxide (NO) (Aktan, 2004).

2.3   Nitric Oxide

Nitric oxide (NO) is an important signalling molecule in the body. Within the vasculature, endothelial nitric oxide synthase (eNOS) catalyses the formation of NO from L-arginine (see **Figure 2.2**). eNOS is dependent upon a number of cofactors including calcium, NADPH and tetrahydrobiopterin (Fleming and Busse, 2003, Fernandez-Sanchez et al., 2011).

Upon synthesis, NO diffuses to the underlying smooth muscle where it activates guanylate cyclase, leading to an increase in cyclic guanosine monophosphate (cGMP). In turn, cGMP activates protein kinase G, thereby opening large conductance potassium channels and reducing intracellular calcium, causing relaxation of the smooth muscle. In this way, NO is a powerful vasodilator that regulates resting blood flow (Andresen et al., 2006).

In addition to its direct vasodilating effects, NO also protects the vasculature by inhibiting leukocyte adhesion to the endothelium, thereby preventing leukocytes from moving into the tissue and evoking an inflammatory response. Moreover, endothelial-derived NO is a potent inhibitor of platelet adhesion. Therefore, when NO bioactivity is reduced, platelets can adhere to the endothelium and form a blood clot, thereby obstructing the flow of blood. Finally, endothelial-derived NO plays a key role in inhibiting vascular growth and hypertrophy, and ensuing vascular functional

impairment (Baumbach et al., 2004). In this way, NO plays a key role in mediating vascular function, inflammation, coagulation pathway and vascular growth.
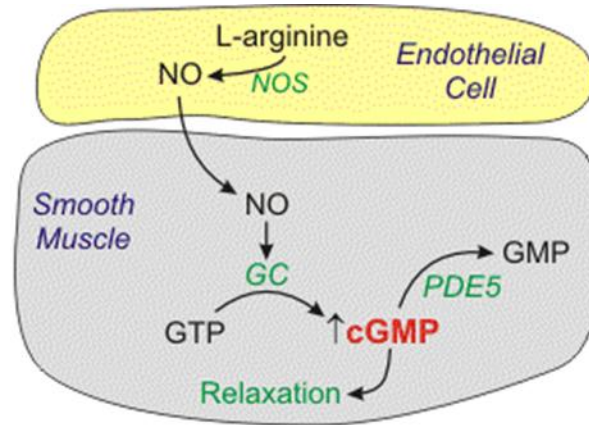
Figure 2.2. Vascular smooth muscle NO-dependent relaxation. Nitric oxide synthesised in endothelial cells diffuses locally through smooth muscle cells and activates guanylate cyclase which increase cGMP and leads to the relaxation of the muscle and vasodilation.

2.3.1 NO Bioavailability

The bioavailability of NO depends upon the balance between NO production and NO inactivation. Oxidative stress decreases NO bioavailability through several mechanisms including (i) enhanced consumption of NO by high levels of superoxide to generate peroxynitrite (Furukawa et al., 2004), inhibition of the enzyme dimethylarginine dimethylaminohydrolase, leading to an increase in asymmetric dimethylarginine, a competitive inhibitor of NO synthesis, (iii) oxidation and depletion of the eNOS cofactor, tetrahydrobiopterin leading to uncoupling of eNOS and (iv) activation of NADPH oxidase which in turn produces more superoxide. A reduction in NO bioavailability leads to impaired endothelium-dependent relaxation of blood vessels, a condition known as endothelial dysfunction.

2.4   Endothelial Dysfunction in Obesity

Obese patients have endothelial dysfunction and decreased vasomotor reactivity (Caballero, 2003). Blunted NO-mediated dilations are well documented in humans (Tesauro et al., 2005) and animals (Erdos et al., 2004) with obesity. Reduced NO-mediated dilations are evident in obese Zucker rats (Katakam et al., 2005) and mice that are fed with high-fat diet (Donato et al., 2012).

Impaired endothelium-dependent dilations will cause a decrease in blood flow and thus a reduction in oxygen supply to the tissue, leading to microvascular complications. Loss of endothelium-dependent vasodilation is predictive of cardiovascular disease (Schachinger et al., 2000) and is a risk factor for dementia, particularly Alzheimer's disease (de la Torre, 2000).

In summary, obesity is associated with vascular inflammation, oxidative stress and endothelial dysfunction. These factors work together to increase patient's risk of developing stroke and Alzheimer's disease.

2.5   Sirtuin 1

Sirtuin 1 (SIRT1) belongs to the sirtuin family of class III histone deacetylases that requires NAD^+ to remove acetyl groups from proteins. SIRT1 helps to regulate many metabolic pathways within the cell. Activation of SIRT1 has been shown to mirror the beneficial effects of calorie restriction (de Ligt et al., 2014). SIRT1 deacetylates a number of proteins, and in doing so, either represses or activates their activity.

2.5.1 SIRT1 Targets PGC-1α

SIRT1 deacetylates peroxisome proliferator-activated receptor γ coactivator-α (PGC-1α), thereby increasing its activity, resulting in greater transcription of nuclear encoded mitochondrial genes (Puigserver et al., 1998). Activation of PGC-1α also induces mitochondrial biogenesis and increased expression of antioxidants such as MnSOD, to prevent an ensuing increase in mitochondrial produced ROS (Valle et al., 2005). PGC-1α is also a co-activator of the nuclear receptor protein, PPAR-α. Inhibition of SIRT1 has been shown to increase PGC-1α acetylation, thereby inhibiting PPAR-α and increasing Nox4-derived superoxide production (Zarzuelo et al., 2013).

2.5.2 SIRT1 Targets eNOS

SIRT1 is known to co-localise with eNOS in the cell, deacetylating lysine residues 496 and 506 in the calmodulin-binding domain, leading to increased eNOS activity (Mattagajasingh et al., 2007). Pharmacological inhibition of SIRT1 decreases eNOS expression level (Zhang et al., 2008) and conversely pharmacological activation increases eNOS expression (Ota et al., 2010). This close relationship between SIRT1 and eNOS, impaired SIRT1 production has been shown to shadow blunted NO-dependent dilations (Hwang et al., 2013).

2.5.3 SIRT1 Targets p53

p53 is a tumor suppressor protein, known as "the guardian of the genome", playing a role in cell cycle regulation. During conditions of oxidative stress, ROS will cause DNA damage. In the event that this DNA damage cannot be fixed by repairing

enzymes, p53 becomes post-transcriptionally modified. This results in the expression of several proteins including p21 or pro-apoptotic genes like BAX, PUMA, and NOXA (Montero et al., 2013). In this way, p53 activity drives cell apoptosis. p53 is a target of SIRT1. Following SIRT1-mediated deacetylation, p53 activity is inhibited, in turn inhibiting p53-dependent apoptosis (Hori et al., 2013, Vaziri et al., 2001).

2.5.4   SIRT1 Targets NCF1

Neutrophil cytosolic factor 1 (NCF1) is a gene coding for p47-phox subunit of NADPH (Li et al., 2005). Overexpression of SIRT1 has been shown to reduce inflammatory responses by regulation of transcription factors such as NCF1 (Hori et al., 2011).

2.5.5   SIRT1 Targets Nox4

As mentioned earlier, Nox4 is a subunit of the NADPH oxidase enzyme complex. Previous studies have shown that inhibition of SIRT1 upregulates the NADPH oxidase subunits, p22phox and Nox4 (Zarzuelo et al., 2013).

2.5.6   SIRT1 Targets p66Shc

Shc proteins are intracellular adaptor proteins that mediate oxidative stress. There are three isoforms in mammalian cells: ShcA (ubiquitously expressed), ShcB and ShC (expressed only in neuronal cells). The ShcA adaptor protein has three isoforms: p46Shc, p52Shc and p66Shc. p66Shc effects ROS production in different ways depending upon its location within the cell. In the nucleus, p66Shc-mediated

inhibition of FOXO transcription factors, cause decreased expression of the antioxidant enzymes, MnSOD and catalase (Nemoto and Finkel, 2002). At the plasma membrane, p66Shc promotes NADPH-membrane oxidase-drive ROS production (Khanday et al., 2006). Within the mitochondria, activation of p66Shc increases ROS production via the mitochondrial electron transport chain (Giorgio et al., 2005). Loss of p66Shc decreases DNA damage, necrosis, and apoptosis (Cosentino et al., 2008). SIRT1 deacetylates pp66Shc, leading to inhibition of p66Shc expression (Zhou et al., 2011).

2.5.7   SIRT1 and 3- Nitrotyrosine

Nitrotyrosine is a product of tyrosine nitration by RNS such as peroxynitrite anion and nitrogen dioxide (see *Oxidative Stress*). Overexpression of SIRT1 has shown to reduce accumulation of nitrotyrosine (Camici et al., 2007).

2.5.8   SIRT1 Targets SOD2

SOD2 is the gene coding for MnSOD protein. SOD2 is one of the three isoforms of SOD (SOD1, SOD2 and SOD3) that is localised to the mitochondria (Weisiger and Fridovich, 1973). SIRT1 enhances the activation of MnSOD through an interaction between PGC-1α and deacetylation of FOXO1 (Olmos et al., 2009).

2.6   Obesity Downregulates SIRT1

Fasting and calorie restriction leads to upregulation of SIRT1 message and protein (Cohen et al., 2004). Conversely, SIRT1 is downregulated in obesity in both humans

(circulating peripheral blood mononuclear cells) (de Kreutzenberg et al., 2010) and animals on a high fat diet (liver and pancreas) (Chen et al., 2010). Our laboratory has shown that SIRT1 is highly expressed in cerebral arteries (Tajbakhsh and Sokoya, 2012) and vascular SIRT1 is downregulated in rats fed a high-fat diet (Tajbakhsh et al, in preparation). Of further interest, SIRT1 genetic variation appears to be associated with increased risk of obesity (Zillikens et al., 2009, Peeters et al., 2008).

2.7   Summary

Obesity increases the risk of cardiovascular disease, stroke and dementia, mainly due to vascular complications. SIRT1 is a protein deacetylase with known antioxidant properties and ability to enhance nitric oxide bioavailability. Mice with targeted disruption of the gene encoding for SIRT1 provide a unique opportunity to examine the role of SIRT1 during high fat feeding. We hypothesized that SIRT1 overexpression would slow down the phenotypes of vascular ageing mediated by high fat feeding, including inflammation, oxidative stress, thereby promoting vascular health.

2.8   Biotechnology Significance of this Study

The academic significance of this project is to identify the potential of targeting SIRT1 in promoting vascular health during high-fat feeding. This project stands as one of the milestones towards identifying a new therapeutic target in patients suffering obesity. Targeting SIRT1 could potentially protect these patients from developing other diseases such as type II diabetes, Alzheimer's disease and stroke.

Currently, resveratrol (a compound known to activate SIRT1) is undergoing clinical trials for its role as an anti-ageing target. Understanding the precise molecular mechanisms of SIRT1 could lead towards the identification of novel drug targets that could be used for personalised and more successful therapies.

3. MATERIALS & METHODS

3.1 Ethics Approval

All animal procedures conformed to the Guide for the Care and Use of Laboratory Animals (National Institutes of Health publication no. 85-23, revised 1996) and were approved by the University of Utah and Veteran's Affairs Medical Center-Salt Lake City (VAMC-SLC) Animal Care and Use Committees. Use of the tissue from these genetically modified organisms has been permitted by the Flinders University Biosafety Committee.

3.2 Animal Model

3.2.1 SIRT1 Transgenic Knock-in Mice

The genetically modified SIRT1 knock-in (SIRT1-KI) mice were generated by knocking in mouse SIRT1 cDNA into the β-actin locus (Bordone et al., 2007).
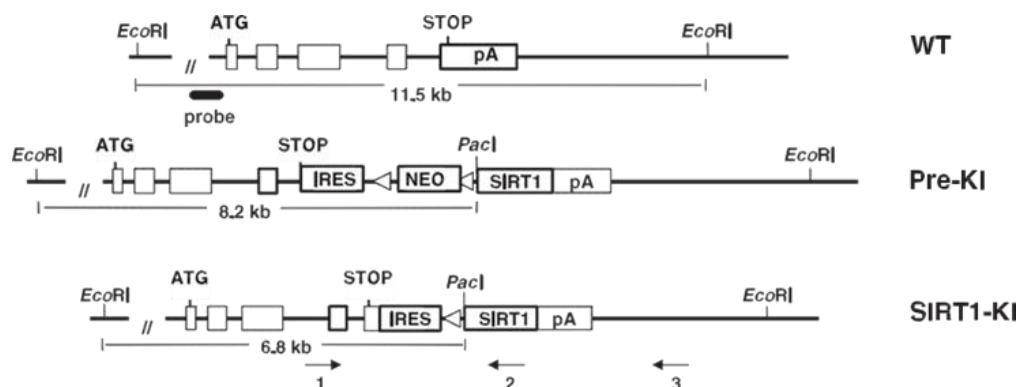
Figure 3.1. Generation of SIRT1 transgenic mice. WT is the genomic organization of the mouse β-actin locus (wildtype), ore-K1 is the preknockin allele in embryonic stem cells and SIRT1-K1 is the SIRT1 expressing allele in mice after removal of neo by Cre recombinase (Bordone et al., 2007).

SIRT1 protein is expressed at higher levels in SIRT1-KI mice compare to wildtype mice. These mice have been previously shown to be leaner, with reduced levels of cholesterol, free fatty acids, and leptin and are more glucose tolerant (Bordone et al., 2007).

Diet Regimen: Male SIRT1-KI (n=18) and B6C57 (wildtype, WT, n=15) mice were bred and housed in the animal facility at VAMC-SLC (University of Utah). Animals were maintained under controlled room temperature with a 12:12 hour light-dark cycle. At 8 months of age, mice were randomly assigned into two groups: high-fat or normal diet (see **Table 3.1**). The high-fat group (HFD) was placed on a high-fat diet (Harlan Teklad custom diet TD.96132) which consisted of 18.7% protein, 40.7% carbohydrate, 40.7% fat (by kcal). The remaining group (NC) was maintained on a control diet (8640 Harlan Teklad 22/5 Standard Rodent Chow) which contained 29% protein, 55% carbohydrate, 16% fat (by kcal). Animals had free access to water and their assigned diets for two months, after which tissues were removed for analysis. Before tissue harvest, mice were euthanized via exsanguinations by cardiac puncture while under isoflurane anesthesia. After collection, all samples were sent to Flinders University in liquid nitrogen.

Table 3.1. Size of Experimental Cohorts contributed in this study.

Genotype	Diet	N
WildType (WT)	Normal Chow (NC)	5
WildType (WT)	High Fat Diet (HFD)	10
SIRT1-K1	Normal Chow (NC)	10
SIRT1-K1	High Fat Diet (HFD)	8

3.3 Blood Glucose Measurement

During anesthesia, blood glucose was measured from the tail vein using an Accu-Chek Performa glucometer and test strips (Roche Diagnostics, Indianapolis, IN, USA).

3.4 Cholesterol, Triglyceride and High-density Lipoprotein Measurements

Blood was obtained by cardiac puncture and collected in lithium heparin tubes (Greiner). After a 10min centrifugation (2000g for 10 minutes), the plasma was carefully removed and collected in a microfuge tube and stored at -20˚C. Cholesterol, triglycerides and high-density lipoprotein (HDL) were measured using an automatic analyser (SA Pathology).

3.5 Message Expression Studies

3.5.1 Extraction of RNA

Whole blood was stored in RNA later (Life Technologies - AM7020) in a ratio of 1:3 and stored at -80°C until it was shipped to Flinders University in liquid nitrogen. Total RNA was extracted from blood using TRI-reagent (Sigma Aldrich - T9424). In a 15 ml polytron tube, 5 ml TRI-reagent was added to 500 µl of thawed blood, mixed by inversion and incubated for 5 minutes at room temperature. 1 ml chloroform was added to the reaction, mixed and incubated for 10 minutes at room temperature. Subsequently, it was centrifuged at 2352 g at 4°C for 15 minutes using a 6K15 Sigma Laboratory Centrifuge. The top aqueous phase containing RNA was transferred to a new polytron tube and 2.5 µl of 2-propanol was added to it. After securing the cap, it

was mixed by inversion and left at room temperature for 8 minutes and centrifuged at 2352 g at 4°C for 1 hour. The supernatant was discarded and 5 ml 75% ethanol was added to the pellet and mixed, followed by 15 minutes centrifugation at 2352 g at 4°C. Finally, the supernatant was discarded and 50 µl of DEPC treated H_2O (Sigma Aldrich - 95284) was added to the pellet. After mixing, the RNA was stored at -80°C.

3.5.2   RNA Purification

The RNA samples were treated with DNase to ensure no genomic DNA was remaining. RNA from each sample was DNase treated using TURBO DNA-*Free*^{TM} Kit (Life Technologies - AM1907). 25 µg total RNA, DEPC treated H_2O to 50 µl, 5 µl 10X TURBO DNase 1 buffer, and 1 µl TURBO DNase 1 enzyme were incubated at 37ºC for 30 minutes. Subsequently, 5.6 µl resuspended DNase inactivation reagent was added and incubated for 2 minutes at room temperature. Finally, samples were centrifuged at 10,000g for 1.5 minutes at room temperature, and DNase free RNA was transferred to a clean tube.

3.5.3   RNA Quantification

RNA quality and concentration were measured using an Agilent 2100 Bioanalyser (Agilent Technologies) and NanoDrop 2000 spectrophotometer (Thermo-Scientific), respectively. The concentration of RNA samples was measured by using 1 µl of the sample and placing it on the pedestal of the NanoDrop. The concentration was measured three times for each sample and their mean value was used.

Subsequently, the quality of the samples was determined by using the Agilent RNA 6000 Pico Kit (Agilent Technologies – 50671513) as per the manufacturer's instruction. RNA samples were diluted to the appropriate concentration ranging between 500 – 5000 pg/µl, as detected by the kit.

3.5.4 cDNA Synthesis

Complementary DNA (cDNA) was synthesised from total RNA using reverse transcriptase (RT). 9 µl total RNA, 1 µl dNTP mix (10 µM), 2 µl random hexamers at 50 ng/µl were added to a 0.5 mL PCR tube and incubated for 5 min at 65°C using an iCycler PCR system (BioRad Laboratories - 583BR). The sample was placed on ice for 2 min, and 4 µl of 5x First Strand buffer (Life Technologies - Y02321), 2 µl 0.1 mM DTT, 1µl RNaseOUT^{TM} Recombinant Ribonuclease Inhibitor (Life Technologies - 10777019) were added and incubated for 2 min at 25°C. 1µl Superscript III Reverse Transcriptase (Life Technologies - 18080044) was added to the sample and incubated for 10 min at 25°C, 50 min at 42°C followed by 15 min at 70°C using the iCycler. DEPC treated H_2O was added to 100 µl. The synthesised cDNA was stored at -20°C.

3.5.5 Real-Time PCR

Real-time PCR, also referred to as quantitative PCR (RT-qPCR), was carried out using a ViiA™ 7 (Applied Biosystems), according to the manufacturer's instructions. Primer sequences were designed in-house by using OligoAnalyzer (version 3.1) available online at Integrated DNA Technology (IDT) website (see **Table 3.2**).

Table 3.2. Primer sequences for Sirt1, Sod1, Ncf1, Sod2, p65 and 18S rRNA genes used in message expression studies.

Primer		Oligonucleotide Sequence in 5'-3' Orientation	Supplier
SIRT1	F	TGA TTG GCA CCG ATC CTC G	Integrated DNA Technologies (IDT)
	R	CCA CAG CGT CAT ATC ATC CAG	
SOD1	F	AAC CAG TTG TGT TGT CAG GAC	
	R	CCA CCA TGT TTC TTA GAG TGA GG	
SOD2	F	CAG ACC TGC CTT ACG ACT ATG G	
	R	CTC GGT GGC GTT GAG ATT GTT	
NCF1	F	ACA CCT TCA TTC GCC ATA TTG C	
	R	TCG GTG AAT TTT CTG TAG ACC AC	
p65	F	ACT GCC GGG ATG GCT ACT AT	
	R	TCT GGA TTC GCT GGC TAA TGG	
18S rRNA	F	GTA ACC CGT TGA ACC CCA TT	
	R	CCA TCC AAT CGG TAG TAG CG	

Commercially available Power SYBR® Green PCR Master Mix (Life Technologies - 4367659) was used to prepare PCR mix. First strand cDNA was synthesized using random hexamer primers. The cycle conditions for real-time PCR were 50°C for 2 min, 95°C for 10 min followed by 45 cycles of 95°C for15 sec, 60°C for 1 min followed by a melt curve of 95°C for 15 sec, 60°C for 1 min and 95°C for 15 sec. All reactions were performed in triplicate and a negative control (H_2O) was included on each PCR plate. At the end of the experiment, the cycle threshold (Ct) values were exported as an Excel data file. PCR products were visualised using polyacrylamide gel electrophoresis.

3.5.6 Polyacrylamide Gel Electrophoresis

RT–PCR amplification products were separated on a 15% TBE Criterion precast (BioRad Laboratories - 3450057) polyacrylamide gel. The gel was placed in the gel tank, filled with 1X TBE buffer made from 10X stock TBE buffer (BioRad Laboratories - 1610733). A 50 bp DNA ladder (BioLabs - N3236S) was prepared per manufacturer specifications. Samples were prepared by addition of 10 μl of the PCR product to 2 μl of 6X DNA gel loading dye which was supplied with the ladder. 10 μl of PCR products and dye mix was loaded on the gel for each sample. Electrophoresis was conducted at 150V constant for 90 minutes. Consequently, the gel was stained for 40 minutes at room temperature using SYBR Green I Nucleic Acid Gel Stain (Invitrogen - S7563) diluted 1:10,000 in 0.5X TBE. The gel image was captured using a BioRad EZ-Doc Imager.

3.5.7 Real-time PCR Analysis

The cycle threshold (Ct) value of the gene of interest (GOI) was normalised to the Ct of 18S rRNA (reference gene). 18S rRNA is a highly abundant and accounts for the majority of RNA. It is one of the most commonly used reference or housekeeping genes for message expression studies. Previous studies have shown that 18s rRNA is a stable internal control and more reliable for high fat diet investigations compared to GAPDH (Sellayah et al., 2008).

Data are expressed as the mean normalised expression calculated using the Pfaffl equation (see **Equation 1**).

$$\textbf{Eq.1} \qquad \text{Mean Normalized Expression} = \frac{E_{GOI}{}^{\Delta CT(GOI-REF)}}{E_{REF}{}^{\Delta CT(GOI-REF)}}$$

This equation calculates the mean normalized expression of the gene of interest (GOI) based on the efficiency (*E*) and the Ct value of the GOI, expressed in relation to the reference gene (REF).

3.6 Protein Studies

3.6.1 Protein Extraction of Carotid Artery Using a Rotor-Stator Homogenizer

Two pieces of carotid arteries were harvested from mice, cleaned of connective tissue and placed in 30 µl of protein extraction buffer without detergent. Samples were snap frozen in liquid nitrogen and stored at -80°C until they were shipped to Flinders University.

On the day of extraction, samples were thawed and placed in either 140 or 160 µl of protein extraction buffer containing 50 mM Tris, pH 8.0 with 2% w/v sodium dodecyl sulfate (SDS), 5 mM dithiothreitol (DTT), and a protease inhibitor tablet (Roche, Indianapolis, IN, USA). The arteries for each cohort were pooled and homogenized (IKA® Ultra Turrax®-T10 homogenizer). After centrifuging for 15 min at 15,000 g, a portion of the supernatant was used for total protein analysis and 10µl aliquots were immediately transferred to -80°C freezer for storage.

3.6.2 Protein Quantification

To determine solubilized protein concentration of mouse carotid artery lysates, total protein content was quantified using EZQ Protein Quantification Assay. Ovalbumin standards were created by serial dilutions of ovalbumin (Life Technologies - R33200) in water to have final concentrations of 2.0, 1.0, 0.5, 0.2, 0.1, 0.05 and 0.02 mg/ml.

These formed the standard curve. Assay results were read with a BioRad EZ-Doc Imager. Analysis was performed by using Carestream Software to determine the protein concentration of the artery lysate.

3.6.3   Western Blotting

Western blotting was used to quantitate SIRT1, eNOS, p53, nitrotyrosine, p66, MnSOD and p21 proteins expression levels. Carotid artery samples were prepared by boiling for 5 min at 95°C with 4X solubilizing buffer (see **Appendix 4**) containing 260 mM dithiothreitol (DTT*)* (Bio-Rad Laboratories). Samples were loaded onto each well of a 4-20 % SDS-PAGE Mini-PROTEIN TGX Stain-Free gel (Bio-Rad Laboratories - 4568093) and separated by SDS-PAGE at 100 V for 1.25 hours. Protein was then transferred to an immunoblot low fluorescence polyvinyldiene fluoride (PVDF) membrane (Bio-Rad Laboratories - 1620264) at 4°C for 1 hours. After blocking with 25ml phosphate buffered saline (PBS), pH 7.4 (Sigma - P3813) containing 5% Blotting-Grade Blocker (Bio-Rad Laboratories - 1706404) and 0.1% Tween-20 (Sigma - P2287) for 1 hour at room temperature. The membrane was exposed to the appropriate primary antibody (see **Table 3.3**) and incubated overnight at 4°C.

Table 3.3. Primary antibodies used to probe against protein of interest.

Name	Dilution	Supplier
Mouse monoclonal anti-SIRT1	1:1000	Abcam - ab110304
Mouse monoclonal anti-eNOS	1:1000	BD Transduction Labs - 610297
Mouse monoclonal anti-3-nitrotyrosine	1:250	Abcam - ab52309
Rabbit monoclonal anti-Nox4	1:1000	Abcam - ab110304
Rabbit polyclonal anti-p21	1:200	Santa Cruz - sc-397
Rabbit polyclonal anti-p66Shc	1:500	Millipore - 06-203
Rabbit polyclonal anti-MnSOD	1:500	Millipore - 06-984

The next day, the blot was washed and incubated in either donkey anti-rabbit secondary antibody conjugated to horseradish peroxide (Jackson ImmunoResearch - 711035152) at 1:10,000 dilution or donkey anti-mouse secondary antibody conjugated to horseradish peroxide (Jackson ImmunoResearch - 715035150) at 1:10,000 dilution for 1 hour at room temperature, followed by washing and developing with either SuperSignal West Femto Maximum Sensitivity substrate (Thermo Scientific - 34095) for 1 minute. Visualisation was performed using a digital imager (Fujifilm LAS-4000). Carestream software was used to quantify the chemiluminescent bands by densitometric analysis. Results were normalised to the total protein loaded on the gel.

3.6.4   Data Analysis

All data are expressed as mean ± standard error of the mean (SEM). Statistical analysis was performed using a two-way ANOVA, followed by a one-way ANOVA since there was an effect only with one factor. Data were analysed using GraphPad Prism software (version 6). Statistical significance was accepted with $P<0.05$.

4. RESULTS

4.1   Phenotypic Assessment of High-Fat Feeding

WT and SIRT1-KI mice fed a high-fat diet for two months showed a comparable weight gain (4.1±1.2g in WT versus 3.2±0.7g in SIRT-KI). There was no difference in terms of weight gain between WT mice on normal chow (31.8±1.2g) and their corresponding SIRT1-KI control mice (29.7±1.6g). Food consumption was recorded over this time, and the average daily food intake was similar between groups (2.0±0.1g in WT versus 2.1±0.1g in SIRT1-KI). White adipose tissue (WAT) mass normalised to total body weight was also similar between WT and SIRT1-KI mice on a normal diet (0.016 in WT versus 0.015 in SIRT-KI). Plasma cholesterol and HDL were both significantly elevated with high-fat feeding, however non-fasting total blood glucose concentration and plasma triglycerides were similar in all groups (see **Table 4.1**).

Table 4.1: Characteristics of SIRT1-KI mice fed normal chow and high fat diet. Data are expressed as mean ± SEM. * P<0.05 versus WT NC mice, [#] P<0.05 versus WT HFD mice, [Ø] P<0.05 versus SIRT1-KI NC mice.

Diet	Normal chow		High fat diet	
Genotype	Wildtype	SIRT1-KI	Wildtype	SIRT1-KI
Blood Glucose (mM)	8.2 ± 1.3	8.1 ± 0.5	8.3 ± 0.5	9.0 ± 0.4
Cholesterol (mM)	2.3 ± 0.2	2.0 ± 0.2	$3.2 \pm 0.3^{*}$	2.9 ± 0.3^{Ø}
Triglycerides (mM)	1.5 ± 0.1	1.2 ± 0.1	1.3 ± 0.1	1.3 ± 0.1
HDL (mM)	1.8 ± 0.2	1.5 ± 0.1	$2.7 \pm 0.3^{*}$	2.3 ± 0.3^{Ø}

4.2 Message Expression Results

4.2.1 RNA Quantification Results

RNA quality and concentration was confirmed by both NanoDrop and Bioanalyser (see **Appendix 1 and 2**). RNA was not used if the RIN<7.0, indicating that the integrity of the RNA was reduced.

4.2.2 Visualisation of PCR Products using Gel Electrophoresis

Gel electrophoresis yielded products of expected size for SIRT1 (86 bp), SOD1 (139 bp), SOD2 (113 bp), NCF1 (130 bp), p65 (126 bp) and 18S rRNA (152 bp) (see **Figure 4.1**) showing the specificity of our primers. No bands were detected in the negative controls, confirming the absence of contamination including non-specific products and primer dimers.
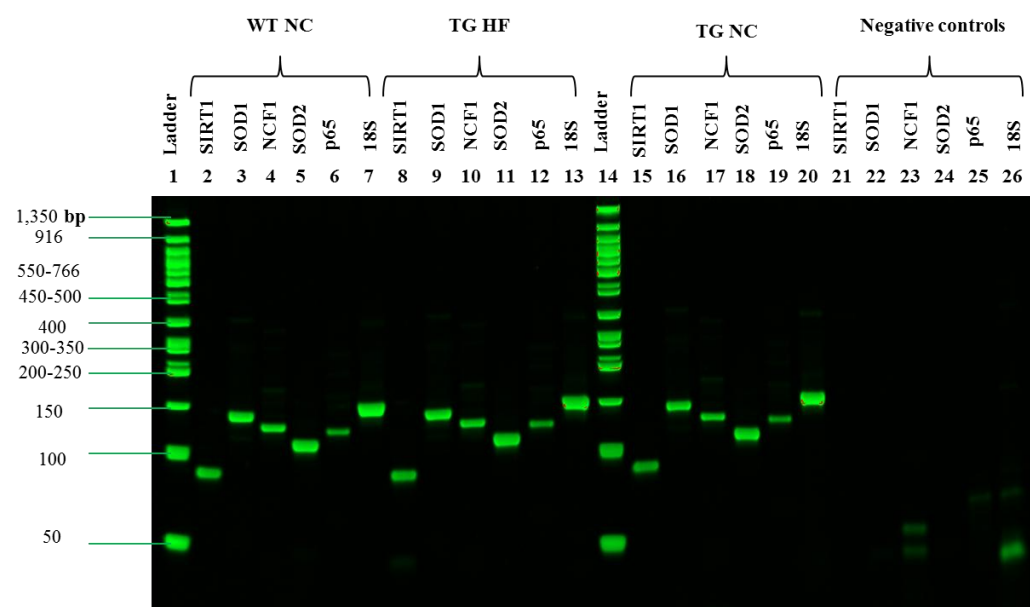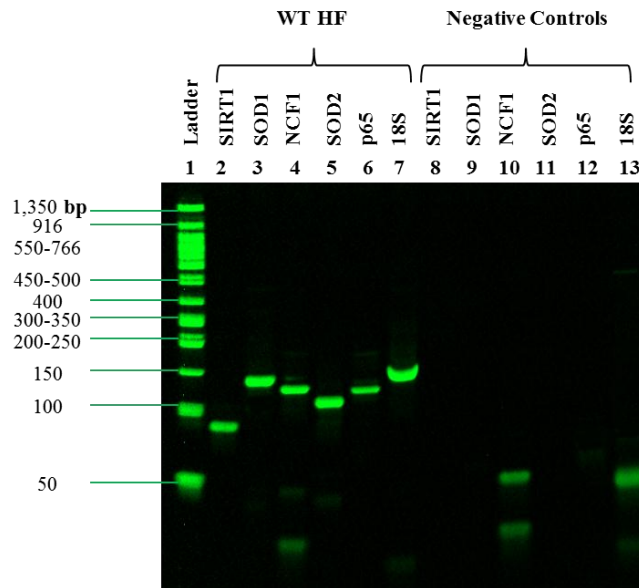
Figure 4.1. Visualisation of PCR products for SIRT1, SOD1, SOD2, NCF1, p65 and 18S rRNA on polyacrylamide gel electrophoresis. As it can be seen all PCR products are within the expected size range. Expected size range for Sirt1, SOD1, Ncf1, SOD2, and p65 and 18S rRNA primers, respectively were 86, 139, 130, 113, 126, and 152 bp.

4.2.3 Real-Time PCR Amplification Efficiencies and Variation

Real-time PCR efficiencies were calculated from the slopes obtained from plotting CT versus cDNA input (ranging from 124 ng to 0.198 ng) for SIRT1 ($E= 1.985$), SOD1 ($E= 1.947$), SOD2 ($E= 1.883$), NCF1 ($E= 1.968$), p65 ($E= 1.935$), and 18S rRNA ($E= 1.87$). Efficiencies were accepted only when $R^2 > 0.998$.

4.2.4 SIRT1 Message Expression in WT versus SIRT1-KI in Blood During High Fat Feeding

SIRT1 mRNA levels were measured in all mice at the end of diet regimen using RT-qPCR. Although there was a trend for increased SIRT1 mRNA expression in SIRT1-KI mice compared to their wildtype controls, this did not reach statistical significance (see **Figure 4.2**). There was also a trend for high-fat feeding to negatively impact SIRT1 message expression in SIRT1-KI mice, but again this was not significantly different.
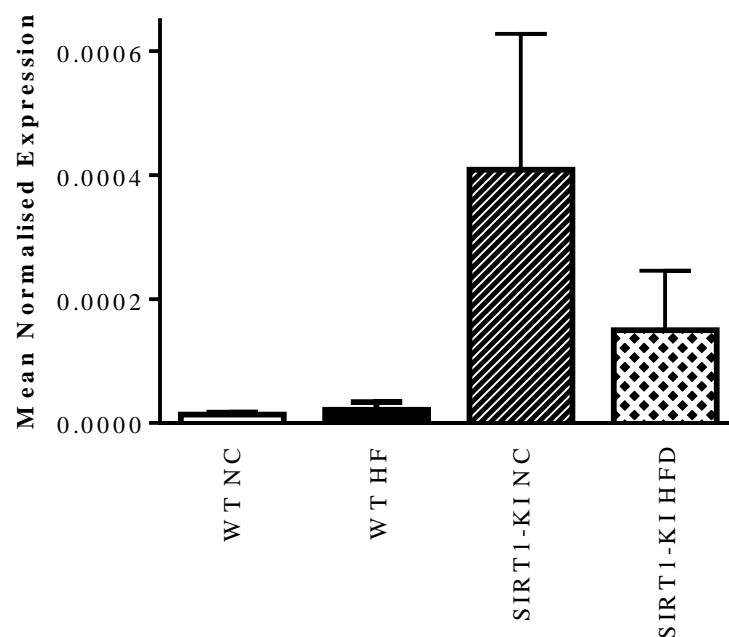
Figure 4.2. Gene expression analysis (RT-qPCR) of SIRT1 from whole blood from WT and SIRT1-KI mice on a ND and HFD (n=6). Data are presented as mean normalised expression of SIRT1 relative to the 18S rRNA housekeeping gene.

4.2.5 SOD1 Message Expression in WT versus SIRT1-KI in Blood During High Fat Feeding

No effect on SOD1 message expression was observed either in response to high-fat feeding or SIRT1 overexpression (see **Figure 4.3**).
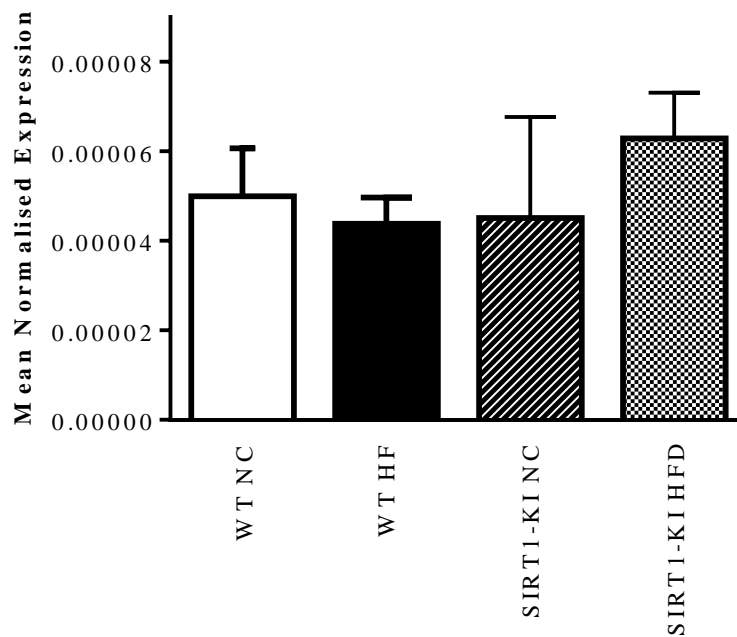
Figure 4.3. Gene expression analysis (RT-qPCR) of SOD1 from whole blood from WT and SIRT1-KI mice on a ND and HFD (n=6). Data are presented as mean normalised expression of SOD1 relative to the 18S rRNA housekeeping gene.

4.2.6 SOD2 Message Expression in WT versus SIRT1-KI in Blood During High Fat Feeding

No effect on SOD2 message expression was observed either in response to high-fat feeding or SIRT1 overexpression (see **Figure 4.4**).
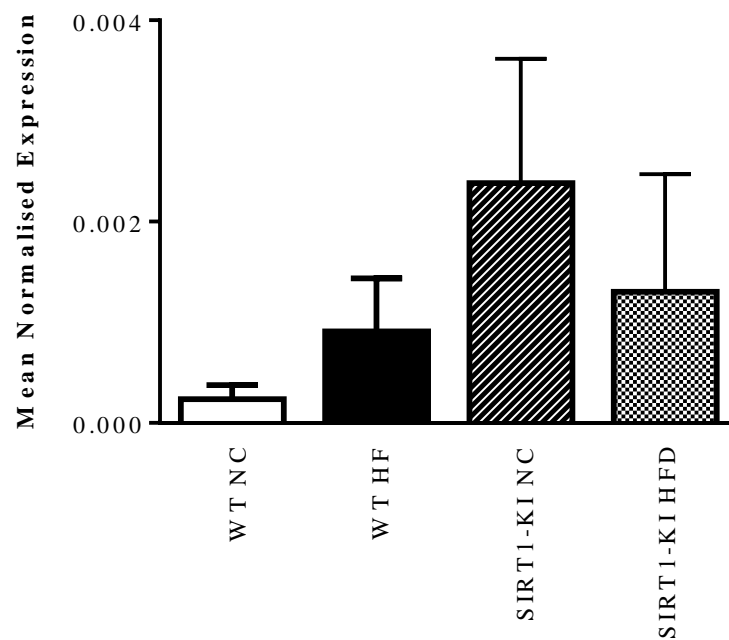
Figure 4.4. Gene expression analysis (RT-qPCR) of SOD2 from whole blood from WT and SIRT1-KI mice on a ND and HFD (n=6). Data are presented as mean normalised expression of SOD2 relative to the 18S rRNA housekeeping gene.

4.2.7 NCF1 Message Expression in WT versus SIRT1-KI in Blood During High Fat Feeding

NCF1 mRNA expression was significantly increased in SIRT1-KI mice on normal chow compared to their wildtype controls (see **Figure 4.5**). There was also a trend for high-fat feeding to negatively impact NCF1 message expression in SIRT1-KI mice, but this did not reach statistical significance.
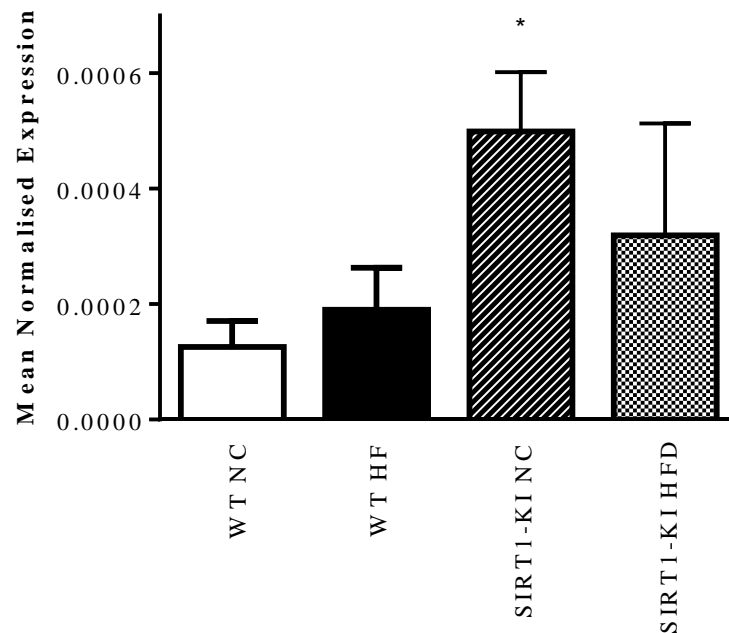
Figure 4.5. Gene expression analysis (RT-qPCR) of NCF1 from whole blood from WT and SIRT1-KI mice on a ND and HFD (n=6). Data are presented as mean normalised expression of NCF1 relative to the 18S rRNA housekeeping gene.

4.3 Protein Expression Results

4.3.1 SIRT1 Protein Expression in WT versus SIRT1-KI Carotid Artery Lysate

Western blotting revealed the presence of a single band at the expected molecular weight of 110 kDa. In WT mice, a high-fat diet significantly decreased carotid artery SIRT1 protein expression compared to normal diet (see **Figure 4.6**). In SIRT-KI mice, carotid artery SIRT1 expression was increased 2.5-fold compared to WT littermates. High-fat feeding did not reduce SIRT1 protein expression in SIRT1-KI mice.
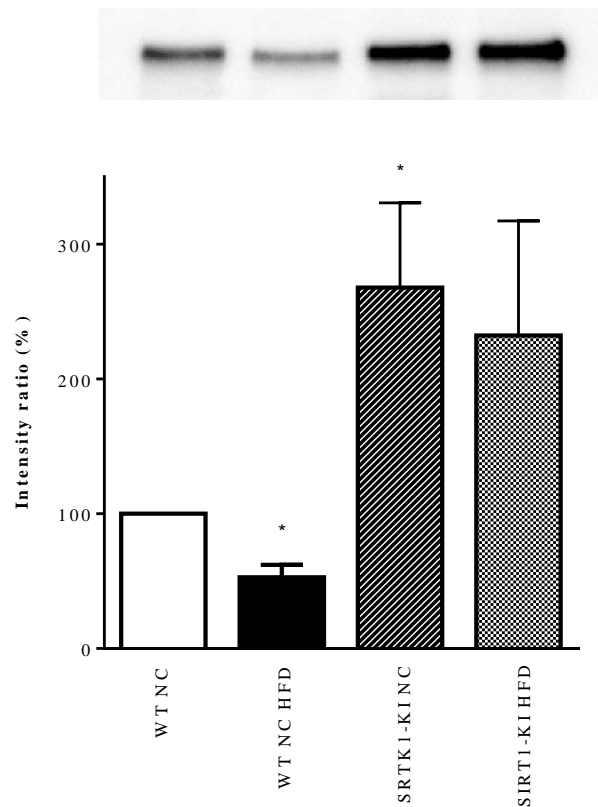
Figure 4.6. Densitometric analysis of SIRT1 protein expression in mouse carotid arteries from WT mice on a normal and high-fat diet and SIRT1-KI mice on a normal and high-fat diet (n=3 in each group; * P<0.05 versus WT NC mice). Data are shown normalised to total protein loaded. Representative Western blots of immunoreactive band intensities showing expression of SIRT1 are shown above the summary data.

4.3.2 eNOS Protein Expression in WT versus SIRT1-KI Carotid Artery Lysate

Western blotting revealed the presence of a single band at the expected molecular weight of 140 kDa. Carotid artery eNOS protein expression was significantly increased in SIRT1-KI on a high-fat diet compared to SIRT1-KI on a normal diet (see **Figure 4.7**).
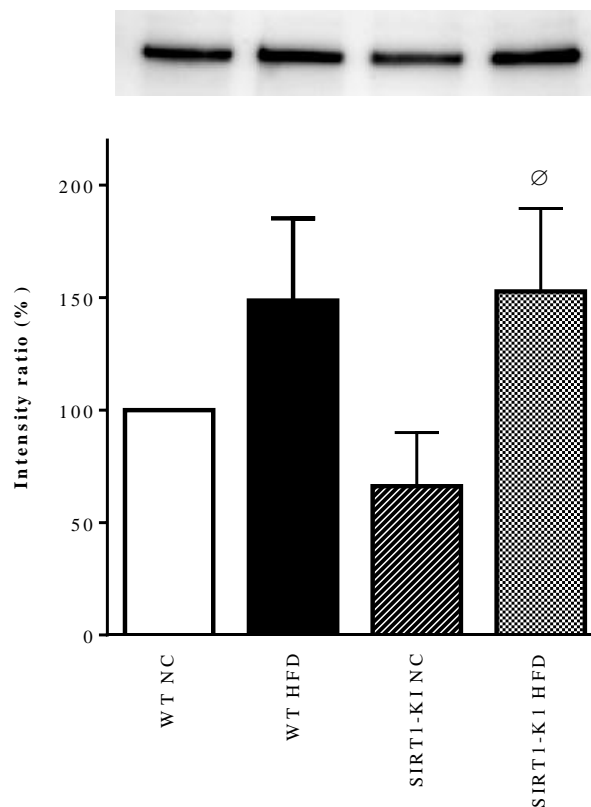
Figure 4.7. Densitometric analysis of eNOS protein expression in mouse carotid arteries from WT mice on a normal and high-fat diet and SIRT1-KI mice on a normal and high-fat diet (n=3 in each group; Ø $P<0.05$ versus SIRT1-KI mice on NC). Data are shown normalized to total protein loaded. Representative Western blots of immunoreactive band intensities showing expression of eNOS are shown above the summary data.

4.3.3 Expression of 3-Nitrotyrosine in WT versus SIRT1-KI Carotid Artery Lysate

In mouse carotid artery homogenates, 3-nitrotyrosine immunoreactive bands (indicative of peroxynitrite production and protein nitration) were observed between 15-150 kDa. Analysis of these bands revealed that 3-nitrotyrosine levels were significantly elevated in wildtype mice fed a high-fat diet compared to wildtype mice fed a normal diet (see **Figure 4.8**). SIRT1-KI mice had significantly lower 3-nitrotyrosine levels compared to wildtype mice and the high-fat-induced increase in 3-nitrotyrosine levels was prevented in SIRT1-KI mice.
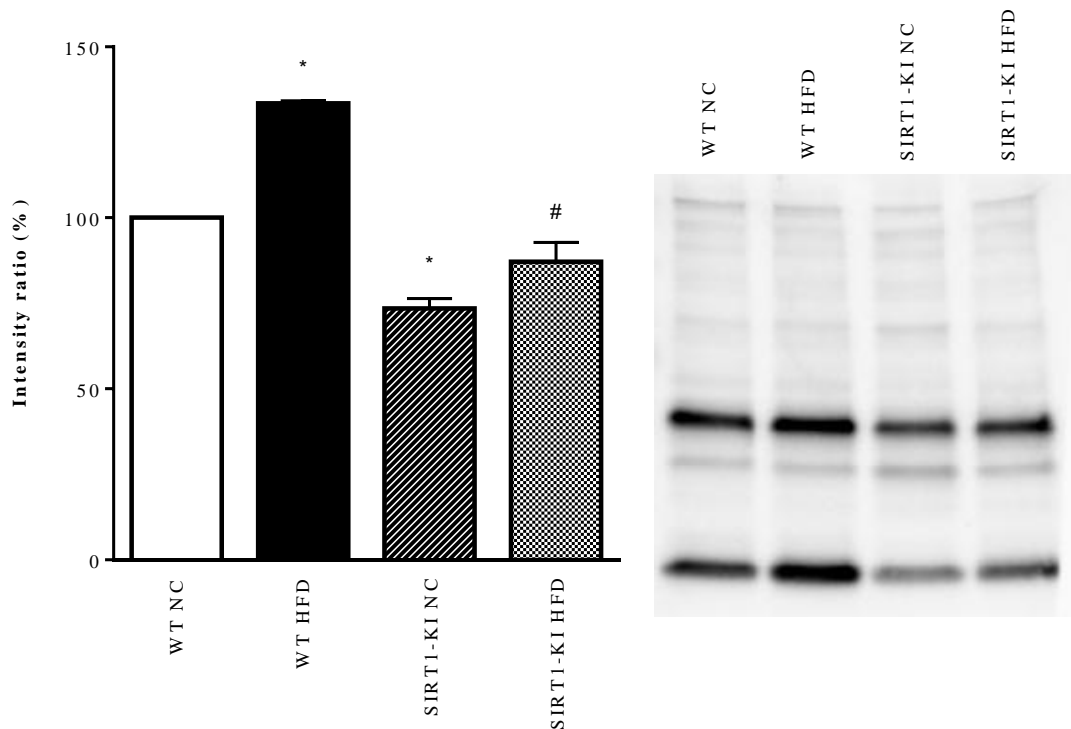
Figure 4.8. Densitometric analysis of 3-nitrotyrosine protein expression in mouse carotid arteries from WT mice on a normal and high-fat diet and SIRT1-KI mice on a normal and high-fat diet (n=3 in each group; * P<0.05 versus WT NC mice; # P<0.05 versus WT HFD mice). Data are shown normalized to total protein loaded. Representative Western blots of immunoreactive band intensities showing expression of 3-nitrotyrosine are shown above the summary data.

4.3.4   Nox4 Protein Expression in WT versus SIRT1-KI Carotid Artery Lysate

Western blotting revealed the presence of a single band at the expected molecular weight of 63 kDa. There was a trend for high-fat feeding to increase Nox4 arterial protein expression in wildtype, but it did not reach statistical difference. There was also a trend for high-fat feeding to negatively impact Nox4 protein expression in SIRT1-KI mice, but again this was not significantly different (see **Figure 4.9**).
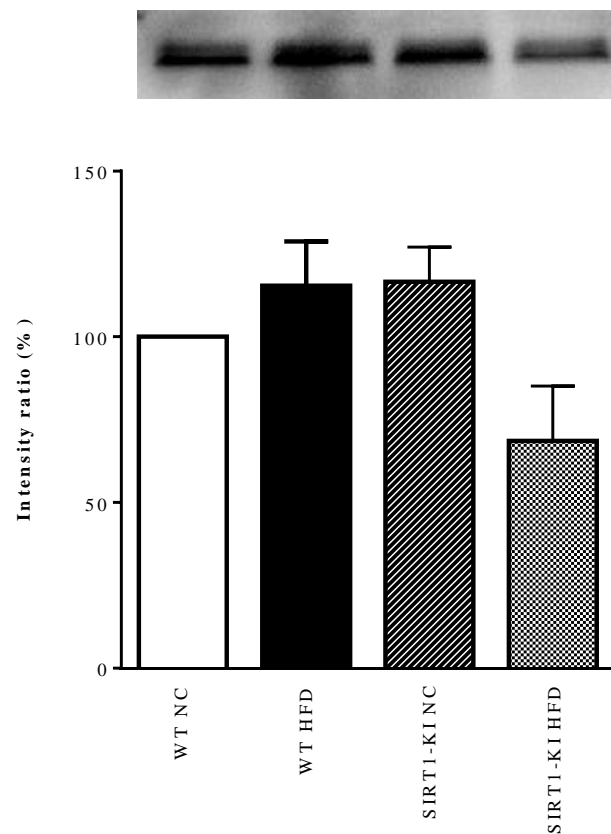
Figure 4.9.   Densitometric analysis of Nox4 protein expression in mouse carotid arteries from WT mice on a normal and high-fat diet and SIRT1-KI mice on a normal and high-fat diet (n=3 in each group). Data are shown normalized to total protein loaded. Representative Western blots of immunoreactive band intensities showing expression of Nox4 are shown above the summary data.

4.3.5 p21 Protein Expression in WT versus SIRT1-KI Carotid Artery Lysate

Western blotting revealed the presence of a single band at the expected molecular weight of 21 kDa. There was a trend for SIRT1 overexpression to increase p21 arterial protein expression, but again it did not reach statistical difference (see **Figure 4.10**).
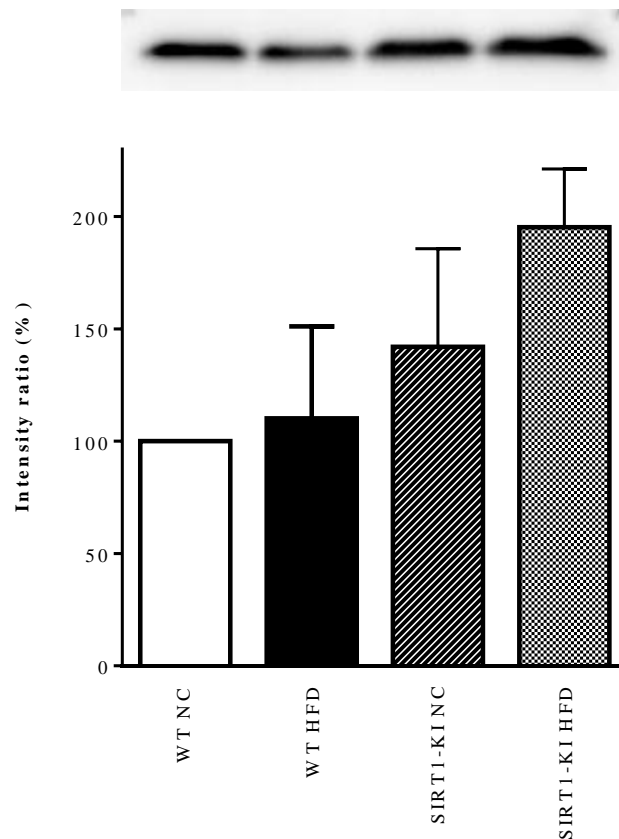
Figure 4.10. Densitometric analysis of p21 protein expression in mouse carotid arteries from WT mice on a normal and high-fat diet and SIRT1-KI mice on a normal and high-fat diet (n=3 in each group). Data are shown normalized to total protein loaded. Representative Western blots of immunoreactive band intensities showing expression of p21 are shown above the summary data.

4.3.6 p66[Shc] Protein Expression in WT versus SIRT1-KI Carotid Artery Lysate

The antibody used in these studies recognises the 46 kDa, 52 kDa and 66 kDa Shc proteins. For the densitometric analysis, we only analysed the 66 kDa band. There was a significant decrease in carotid artery p66 protein expression in SIRT1-KI mice compared to WT controls (see **Figure 4.11**).
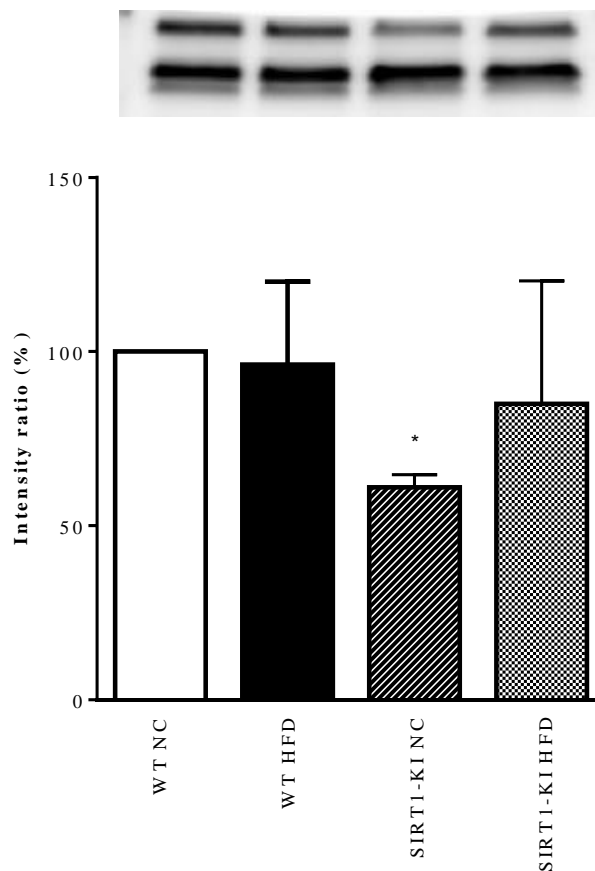
Figure 4.11. Densitometric analysis of p66[Shc] protein expression in mouse carotid arteries from WT mice on a normal and high-fat diet and SIRT1-KI mice on a normal and high-fat diet (n=3 in each group; * $P<0.05$ versus WT NC mice). Data are shown normalized to total protein loaded. Representative Western blots of immunoreactive band intensities showing expression of p66[Shc] are shown above the summary data.

4.3.7 MnSOD Expression in WT versus SIRT1-KI Carotid Artery Lysate

Western blotting revealed the presence of a single band at 24 kDa. With a normal diet, SIRT1 overexpression significantly decreased carotid artery MnSOD protein expression compared to WT controls. However with high-fat feeding this was no longer statistically different (see **Figure 4.12**).
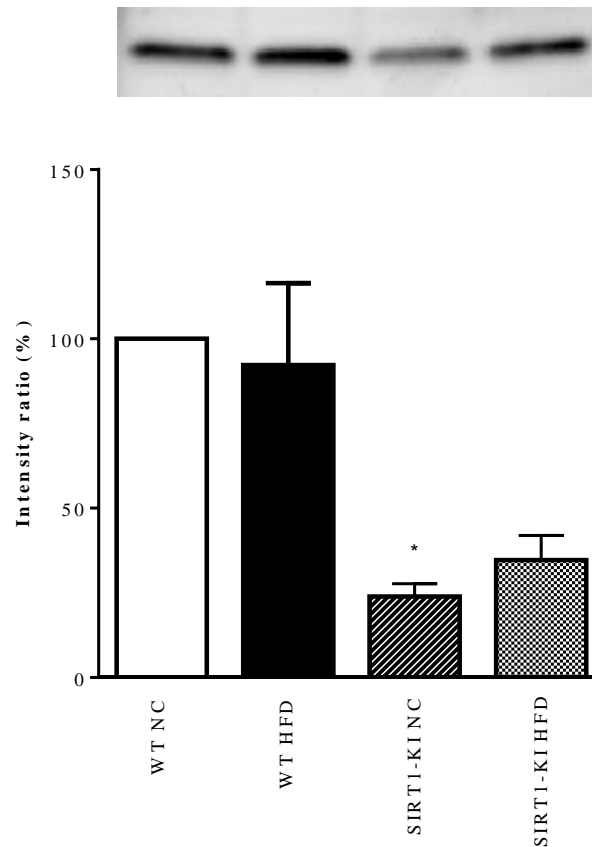
Figure 4.12. Densitometric analysis of MnSOD protein expression in mouse carotid arteries from WT mice on a normal and high-fat diet and SIRT1-KI mice on a normal and high-fat diet (n=3 in each group; * P<0.05 versus WT NC mice). Data are shown normalized to total protein loaded. Representative Western blots of immunoreactive band intensities showing expression of MnSOD are shown above the summary data.

5. DISCUSSION

5.1 Phenotype Characteristics

5.1.1 Weight

Since SIRT1 has been shown to regulate fat metabolism by interacting with PPAR-γ to inhibit the production of new adipocytes (Picard et al., 2002), it is possible that overexpressing SIRT1 would result in leaner animals. We found that WT and SIRT1-KI mice fed normal chow had comparable body weights at 10 months of age. Interestingly, this is in contrast to a report by Bordone and colleagues, using the identical SIRT1-KI mouse model, who showed that SIRT1-KI mice were leaner than WT controls (Bordone et al., 2007). However, in agreement with our studies, other groups have shown comparable weights, using mice that overexpress SIRT1 from a bacterial artificial chromosome (BAC) construct (Pfluger et al., 2008, Banks et al., 2008). We also found that white adipose tissue mass normalised to total body weight was comparable between SIRT1-KI mice and their WT littermates, indicating that the accumulation of fat was comparable between the two groups.

After 2 months on a high-fat diet, there was a trend towards lower body weight in SIRT1-KI mice compared to WT controls (3.2±0.7g versus 4.1±1.2g, respectively). However, this did not reach statistical significance. Of note, similar weight gain following high-fat feeding has been reported using other SIRT1-KI mouse models (Pfluger et al., 2008, Banks et al., 2008). Pfluger and colleagues showed that 4.5 months of high-fat feeding was required before body weight differences were detected (Pfluger et al., 2008). Therefore, it is certainly possible that extending the amount of

time on the diet regimen may result in a significantly lower body weight in SIRT1-KI compared to WT controls.

5.1.2 Average Daily Food Intake

Because SIRT1 has been shown to influence metabolic rate (Bordone et al., 2007) we determined daily food intake in SIRT-KI and WT mice on a high-fat diet. Daily food intake was similar in SIRT1-KI and WT control mice. Pfluger and colleagues (Pfluger et al., 2008) have shown increased food intake in SIRT1-KI mice on a high-fat; however this was only observed with chronic exposure to high-fat feeding (4.5months) and not at 2 months (the end-point in our study). It is possible that we would have seen comparable results if the animals had been followed for a longer time.

5.1.3 Cholesterol and HDL

Although there was a trend for plasma cholesterol and HDL levels to be lower in SIRT1-KI mice than in WT controls, this did not reach statistical significance (see **Table 4.1**). Previous studies have shown that SIRT1 alters cholesterol biosynthesis in the liver and macrophages (Li et al., 2007) by deacetylating liver X receptor, thereby mediating cholesterol homeostasis (Li et al., 2007). It is possible that we are only seeing subtle differences because overexpression of SIRT1 is absent in the liver in these mice (Bordone et al., 2007). Therefore any changes may only reflect subtle changes in cholesterol uptake in the peripheral tissues.

Two months of high-fat feeding resulted in significantly increased plasma cholesterol and HDL levels in both WT mice and SIRT1-KI (compared to normal chow). Similar trends in plasma cholesterol levels have been reported using other SIRT1-KI mouse models (Pfluger et al., 2008) (Banks et al., 2008).

5.1.4 Non-Fasting Glucose and Triglycerides

WT and SIRT1-KI mice on a normal diet had comparable measures of non-fasting plasma glucose. However it is possible that fasting levels of glucose are different between the groups. Indeed, Bordone and colleagues have shown that fasting, but not non-fasting, plasma glucose levels are lower in SIRT1-KI compared to WT mice (Bordone et al., 2007). SIRT1 has been shown to inhibit uncoupling protein 2 (UCP2) transcription in pancreatic beta cells, thereby enhancing insulin secretion (Bordone et al., 2007). This increases the rate of glucose transport into fat and muscle cells, leaving behind lower levels of circulating blood glucose levels.

We also found that plasma triglyceride levels were similar in WT and SIRT-KI mice fed a normal diet or a high-fat diet. SIRT1 has been shown to control triglyceride synthesis in the liver, through activation of SREBP1 (Li et al., 2005). Our finding that overexpression of SIRT1 had no effect on triglyceride concentration may again be a reflection of the lack of liver SIRT1 overexpression in these mice.

5.2 Effect of High-Fat Feeding and SIRT1 Overexpression

5.2.1 High-Fat Feeding Decreases Carotid Artery SIRT1 Protein Expression in WT Mice

SIRT1 protein expression was significantly blunted in carotid artery lysate from WT mice after a high-fat diet compared to a normal diet (see **Figure 4.6**). Few groups have looked at the vasculature. However, Zhang and colleagues reported a decline in mouse aorta SIRT1 protein expression after 6 months on a high-fat diet (Zhang et al., 2008). This is also in line with recent findings from our laboratory that showed decreased cerebral artery SIRT1 protein expression in a rat model of type II diabetes (Tajbakhsh et al, in preparation).

The decrease in vascular SIRT1 protein expression was not paralleled by systemic SIRT1 changes in gene expression (see **Figure 4.2**). There was, however, a high degree of variability between sample replicates therefore increasing sample size in future experiments, may show differential expression between the two cohorts. Indeed, clinical studies have shown an association between metabolic syndrome and low levels of SIRT1 gene and protein expression in peripheral blood mononuclear cells (de Kreutzenberg et al., 2010).

5.2.2 Carotid Artery SIRT1 Expression Is Upregulated in SIRT1-KI Mice

Carotid artery SIRT1 protein expression was elevated 2.5-fold in SIRT1-KI compared to WT mice on a control diet (see **Figure 4.6**). This is the first report showing vascular SIRT1 overexpression in this mouse model. It is line with reports of elevated SIRT1 protein expression in adipose tissue, brain and calvaria cells of the skull in this

mouse model (Bordone et al., 2007). Although there was a trend for SIRT1 gene expression to be elevated in whole blood, this again did not reach statistical significance. Importantly, overexpression of SIRT1 prevented the decrease in SIRT1 protein expression in response to high-fat feeding.

5.2.3 No Effect of High-Fat Feeding on Carotid Artery eNOS Protein Expression

Comparison of WT mice on a normal and high-fat diet, showed similar levels of carotid artery eNOS protein expression, although there did appear to be a non-significant trend towards enhanced protein expression (see **Figure 4.7**). Other studies in both humans and animal models of obesity (Schachinger et al., 2000) have also shown increased eNOS protein expression. This could be occurring by the direct activation of eNOS by insulin (Kuboki et al., 2000) and/or hydrogen peroxide (Kumar et al., 2009). It is important to note that eNOS protein levels are not always associated with NO bioavailability. Indeed, our collaborator Dr Anthony Donato at the University of Utah has shown that endothelium-dependent vasodilation is significantly impaired in mice after 2 months of high-fat feeding, as assessed by stimulation with acetylcholine (personal communication).

5.2.4 High-Fat Feeding Increases Carotid Artery eNOS Protein Expression in SIRT1-KI

On a normal diet, carotid artery eNOS protein levels were similar in SIRT1-KI mice and their WT counterparts. Although pharmacological activation of SIRT1 has been shown to increase eNOS expression (Ota et al., 2007), this was not observed in our study by genetically overexpressing SIRT1. However carotid artery eNOS protein

expression was significantly increased in SIRT1-KI mice after feeding with high-fat diet compared to a normal diet. Assuming that NO bioavailability is not impacted, these results suggest that upregulation of SIRT1 improves carotid artery endothelial function under hypercholesterolaemic conditions. In line with this idea, Dr Anthony Donato has shown preserved endothelium-dependent responses in SIRT1-KI mice after high-fat feeding (personal communication).

5.2.5 High-Fat Feeding Increases Carotid Artery Nitrotyrosine Protein Expression

High-fat feeding was associated with significantly higher levels of protein tyrosine nitration (see **Figure 4.8**). These data suggest that in our model of high-fat feeding in the mouse, peroxynitrite is being formed within the carotid artery, thereby causing nitration of tyrosine residues on proteins. Thus the impairment of endothelial function during high-fat feeding can be mediated in part by inactivation of NO by peroxynitrite-derived superoxide.

5.2.6 Carotid Artery Nitrotyrosine Expression Is Downregulated in SIRT1-KI Mice

Comparison of mice on a normal diet, showed significantly lower levels of 3-nitrotyrosine in carotid arteries from SIRT1-KI mice compared to their WT littermates (see **Figure 4.8**). Importantly, high-fat diet-induced increase in nitrotyrosine expression was prevented in SIRT1-KI mice. This lends support to the idea that SIRT1 protects the vasculature against oxidative stress.

5.2.7 No Effect of High-Fat Feeding on Carotid Artery Nox4 Expression

The expression of Nox4 protein, the catalytic subunit of an isoform of NADPH oxidase, was evaluated in carotid artery homogenate in normal and high-fat diet. Although there was a trend for increased Nox4 protein expression in carotid artery, this did not reach statistical significance (see **Figure 4.9**). Therefore, in our mouse model of high-fat feeding, vascular oxidative stress does not appear to result from Nox4-driven ROS production.

Previous studies have shown a three-fold increase in Nox4 protein expression in rat aorta in high-fat feeding (Jiang et al., 2011). While species (mouse versus rat) and artery (carotid artery versus aorta) differences in Nox4 expression could account for the disparity, it should also be noted that the intensity of the chemiluminescent protein bands were not ideal for densitometric analysis, suggesting that Nox4 protein expression is not highly expressed in the mouse carotid artery. Nox2 protein expression could be evaluated in future experiments, since Nox2 has been shown to be highly expressed in the endothelium (Miller et al., 2007).

5.2.8 No Effect of SIRT1 Overexpression on Carotid Artery Nox4 Protein Expression

Comparison of WT and SIRT-KI mouse aorta on a normal diet, showed that overexpression of SIRT1 had no effect on carotid artery Nox4 protein expression (see **Figure 4.9**). After high-fat feeding, there appeared to be a decline in Nox4 protein expression in SIRT1-KI mice, however this did not reach statistical significance. In line with our results, a recent study has shown that pharmacological activation of SIRT1 had no effect on Nox4 protein expression in the aging mouse aorta (Roos et

al., 2013). Interestingly, whole blood gene expression of NCF1 (p47-phox), a cytosolic component of the NADPH oxidase complex, was significantly elevated in SIRT1-KI mice compared to WT mice on a normal diet (see **Figure 4.5**). It is unclear why NADPH oxidase is upregulated systemically in SIRT1-KI mice; however this was restored in high-fat feeding.

5.2.9 High-Fat Feeding Had No Effect on Carotid Artery p66Shc Protein Expression in WT Mice

Carotid artery p66Shc protein expression was comparable in WT mice on a normal or high-fat diet (see **Figure 4.11**). Upregulation of p66Shc protein has been reported in streptozotocin-treated mice (Camici et al., 2007, Chen et al., 2012) and in cell culture (Malhotra et al., 2009). Therefore the lack of upregulation of p66Shc in our model of high-fat feeding could be due to the absence of overt hyperglycaemia. Indeed, glucose appears to be an important trigger of p66Shc-driven ROS production (Paneni et al., 2012, Sun et al., 2010). Alternatively, the main source of ROS within the vasculature during high-fat feeding may not be mitochondrial, but rather derived from NADPH oxidase. Of note, NADPH oxidase is a particularly important source of ROS in the brain vasculature (Miller et al., 2005).

5.2.10 Carotid Artery p66Shc Protein Expression Is Downregulated in SIRT1-KI Mice

Overexpression of SIRT1 significantly decreased carotid artery p66Shc protein expression, compared to WT mice on a normal diet (see **Figure 4.11**). This data is in line with previous studies showing that SIRT1 binds to the p66Shc promoter, thereby inhibiting p66Shc gene transcription (Zhou et al., 2011). Since p66Shc is an important

source of ROS, downregulation of p66^{Shc} in SIRT-KI mice would potentially translate into reduced DNA damage.

Interestingly, this protection was lost upon high-fat feeding as evinced by comparable p66Shc protein expression levels in WT and SIRT-KI. These data suggest that factors aside from SIRT1 are controlling p66Shc protein expression during high-fat feeding. Interestingly, previous studies have shown that adenoviral overexpression of SIRT1 blocks high glucose-induced p66Shc upregulation in cell culture (Zhou et al., 2011). However our data suggest that transgenic overexpression of SIRT1 does not prevent changes in p66Shc expression in the context of high-fat feeding.

5.2.11 High-Fat Feeding Had No Effect on Carotid Artery MnSOD Protein Expression in WT Mice

As another marker of oxidative stress, protein expression of the antioxidant enzyme, MnSOD was measured in WT mice upon high-fat feeding. Under conditions of significant oxidative stress, one may expect reduced expression of ROS-scavenging enzymes. However in our studies, MnSOD protein expression in WT carotid arteries was comparable in normal and high-fat feeding (see **Figure 4.12**). This may again be a reflection of the length of diet or the lack of overt hyperglycaemia, since recent studies in our laboratory have shown a significant decline in MnSOD protein expression in a model of type II diabetes (Tajbakhsh et al, in preparation).

Although it was expected to see an up regulation of SOD1 gene upon SIRT overexpression due to its antioxidant characteristics, neither upregulation of SIRT1 or diet seemed to have an effect on SOD1 gene expression.

5.2.12 Carotid Artery MnSOD Protein Expression Is Downregulated in SIRT1-KI Mice

Overexpression of SIRT1 significantly decreased carotid artery MnSOD protein expression; compared to WT mice on a normal diet (see **Figure 4.12**). This result was unexpected given that fact that adenoviral overexpression of SIRT1 has been shown to increase MnSOD protein expression (Olmos et al., 2013). Nevertheless, previous studies have shown that SIRT1 upregulation promotes Akt activation (Ota et al., 2010) and chronic Akt activation has been shown to reduce MnSOD concentration (Wang et al., 2009) Future studies would need to address whether Akt is activated in order to confirm this rationale. Interestingly, there was a trend for an increase in whole blood SOD2 gene expression; however this did not reach statistical significance (see **Figure 4.4**). Although carotid artery MnSOD protein expression appeared to be reduced in SIRT1-KI mice on a high-fat diet, this was not statistically different from WT controls on a high-fat diet.

5.2.13 High-Fat Feeding Had No Effect on Carotid Artery p21 Protein Expression in WT Mice

Increased oxidative stress can induce DNA damage, leading to activation of p53 and p21, and cellular senescence. p21 is a well established marker of cellular senescence and some studies have shown that high-fat feeding leads to vascular senescence (Wang et al., 2009). However, we found no effect of high-fat feeding on p21 protein expression in carotid artery lysate in WT mice (see **Figure 4.10**). It is possible that the percentage of fat in this diet (40% in our study versus 60% in the cited paper) or the length of time on the diet (2 months in our study versus 5 months in the cited paper) was insufficient to observe these changes. In support of this idea, Chen and colleagues

found that p21 expression levels were unchanged in aorta of 8-week streptozotocin-treated mice, but they were significantly increased after 40 weeks (Chen et al., 2012). We did attempt to measure p53 protein expression using Western blotting, however we were unsuccessful in obtaining protein bands that were of sufficient intensity to carry out densitometric analysis.

5.2.14 No Effect of SIRT1 Overexpression on Carotid Artery p21 Protein Expression

As expected, overexpression of SIRT1 had no effect on p21 protein expression in carotid artery (when comparing WT and SIRT1-KI on normal diet) (see **Figure 4.4**). This is in accordance with results obtained by Chen and colleagues (Chen et al., 2012). Because high-fat feeding had no effect on p21 expression, there was no benefit observed in SIRT1-KI mice. In future studies it would be important to induce vascular senescence by keeping the mice on the diet for an extended period of time and/or increasing the fat content of their diet, and only then would we be able to determine whether SIRT1 overexpression offers any protection.

6. CONCLUSION

High-fat feeding is known to promote oxidative stress and decreased nitric oxide bioavailability that increases risk of developing stroke or dementia. Sirtuin 1 (SIRT1) is a protein deacetylase with known antioxidant properties and ability to enhance nitric oxide bioavailability. Although SIRT1 activators, such as resveratrol, appear to promote vascular health, they are notoriously promiscuous.

The purpose of the present study was to test the hypothesis that specific SIRT1 overexpression during high-fat feeding would attenuate the phenotypes of vascular ageing such as oxidative stress.

Here we have shown that mice fed a high-fat diet for two months developed significantly elevated levels of plasma cholesterol and HDL. Carotid artery protein expression of SIRT1 was significantly decreased and nitrotyrosine, a marker of oxidative stress, was significantly increased. SIRT1 overexpression prevented these changes in SIRT1 and nitrotyrosine in response to high-fat feeding and also enhanced eNOS protein expression, a marker of endothelial function.

Our results highlight the potential benefits of targeting SIRT1 as a therapeutic strategy in reducing the clinical complications associated with vascular impairment during high-fat feeding.

7. REFERENCES

AKTAN, F. 2004. iNOS-mediated nitric oxide production and its regulation. *Life Sci,* 75, 639-53.

ANDRESEN, J., SHAFI, N. I. & BRYAN, R. M., JR. 2006. Endothelial influences on cerebrovascular tone. *J Appl Physiol (1985),* 100, 318-27.

BABIOR, B. M., KIPNES, R. S. & CURNUTTE, J. T. 1973. Biological defense mechanisms. The production by leukocytes of superoxide, a potential bactericidal agent. *J Clin Invest,* 52, 741-4.

BANKS, A. S., KON, N., KNIGHT, C., MATSUMOTO, M., GUTIERREZ-JUAREZ, R., ROSSETTI, L., GU, W. & ACCILI, D. 2008. SirT1 gain of function increases energy efficiency and prevents diabetes in mice. *Cell Metab,* 8, 333-41.

BAUMBACH, G. L., SIGMUND, C. D. & FARACI, F. M. 2004. Structure of cerebral arterioles in mice deficient in expression of the gene for endothelial nitric oxide synthase. *Circ Res,* 95, 822-9.

BECKER, L. B. 2004. New concepts in reactive oxygen species and cardiovascular reperfusion physiology. *Cardiovascular research,* 61, 461-470.

BORDONE, L., COHEN, D., ROBINSON, A., MOTTA, M. C., VAN VEEN, E., CZOPIK, A., STEELE, A. D., CROWE, H., MARMOR, S., LUO, J., GU, W. & GUARENTE, L. 2007. SIRT1 transgenic mice show phenotypes resembling calorie restriction. *Aging Cell,* 6, 759-67.

BRAY, G. A. & YORK, D. A. 1971. Genetically transmitted obesity in rodents. *Physiol Rev,* 51, 598-646.

BUETTNER, R., SCHOLMERICH, J. & BOLLHEIMER, L. C. 2007. High-fat diets: modeling the metabolic disorders of human obesity in rodents. *Obesity (Silver Spring),* 15, 798-808.

CABALLERO, A. E. 2003. Endothelial dysfunction in obesity and insulin resistance: a road to diabetes and heart disease. *Obes Res,* 11, 1278-89.

CAMICI, G. G., SCHIAVONI, M., FRANCIA, P., BACHSCHMID, M., MARTIN-PADURA, I., HERSBERGER, M., TANNER, F. C., PELICCI, P., VOLPE, M., ANVERSA, P., LUSCHER, T. F. & COSENTINO, F. 2007. Genetic deletion of p66(Shc) adaptor protein prevents hyperglycemia-induced endothelial dysfunction and oxidative stress. *Proc Natl Acad Sci U S A,* 104, 5217-22.

CHEN, H., WAN, Y., ZHOU, S., LU, Y., ZHANG, Z., ZHANG, R., CHEN, F., HAO, D., ZHAO, X., GUO, Z., LIU, D. & LIANG, C. 2012. Endothelium-specific SIRT1 overexpression inhibits hyperglycemia-induced upregulation of vascular cell senescence. *Sci China Life Sci,* 55, 467-73.

CHEN, Y. R., FANG, S. R., FU, Y. C., ZHOU, X. H., XU, M. Y. & XU, W. C. 2010. Calorie restriction on insulin resistance and expression of SIRT1 and SIRT4 in rats. *Biochem Cell Biol,* 88, 715-22.

CODONER-FRANCH, P., TAVAREZ-ALONSO, S., MURRIA-ESTAL, R., MEGIAS-VERICAT, J., TORTAJADA-GIRBES, M. & ALONSO-IGLESIAS, E. 2011. Nitric oxide production is increased in severely obese children and related to markers of oxidative stress and inflammation. *Atherosclerosis,* 215, 475-80.

COHEN, H. Y., MILLER, C., BITTERMAN, K. J., WALL, N. R., HEKKING, B., KESSLER, B., HOWITZ, K. T., GOROSPE, M., DE CABO, R. & SINCLAIR, D. A. 2004. Calorie restriction promotes mammalian cell survival by inducing the SIRT1 deacetylase. *Science,* 305, 390-2.

COSENTINO, F., FRANCIA, P., CAMICI, G. G., PELICCI, P. G., LUSCHER, T. F. & VOLPE, M. 2008. Final common molecular pathways of aging and cardiovascular disease: role of the p66Shc protein. *Arterioscler Thromb Vasc Biol,* 28, 622-8.

DAHIYA, P., KAMAL, R., GUPTA, R., BHARDWAJ, R., CHAUDHARY, K. & KAUR, S. 2013. Reactive oxygen species in periodontitis. *J Indian Soc Periodontol,* 17, 411-6.

DE KREUTZENBERG, S. V., CEOLOTTO, G., PAPPARELLA, I., BORTOLUZZI, A., SEMPLICINI, A., DALLA MAN, C., COBELLI, C., FADINI, G. P. & AVOGARO, A. 2010. Downregulation of the longevity-associated protein sirtuin 1 in insulin resistance and metabolic syndrome: potential biochemical mechanisms. *Diabetes,* 59, 1006-15.

DE LA TORRE, J. C. 2000. Impaired cerebromicrovascular perfusion. Summary of evidence in support of its causality in Alzheimer's disease. *Ann N Y Acad Sci,* 924, 136-52.

DE LIGT, M., TIMMERS, S. & SCHRAUWEN, P. 2014. Resveratrol and obesity: Can resveratrol relieve metabolic disturbances? *Biochim Biophys Acta.*

DONATO, A. J., HENSON, G. D., MORGAN, R. G., ENZ, R. A., WALKER, A. E. & LESNIEWSKI, L. A. 2012. TNF-alpha impairs endothelial function in adipose tissue resistance arteries of mice with diet-induced obesity. *Am J Physiol Heart Circ Physiol,* 303, H672-9.

ERDOS, B., SNIPES, J. A., MILLER, A. W. & BUSIJA, D. W. 2004. Cerebrovascular dysfunction in Zucker obese rats is mediated by oxidative stress and protein kinase C. *Diabetes,* 53, 1352-9.

EVANS, J. L., GOLDFINE, I. D., MADDUX, B. A. & GRODSKY, G. M. 2002. Oxidative stress and stress-activated signaling pathways: a unifying hypothesis of type 2 diabetes. *Endocr Rev,* 23, 599-622.

EYRE, H., KAHN, R. & ROBERTSON, R. M. 2004. Preventing cancer, cardiovascular disease, and diabetes: a common agenda for theAmerican Cancer Society, the American Diabetes Association, and the American Heart Association. *CA Cancer J Clin,* 54, 190-207.

FERNANDEZ-SANCHEZ, A., MADRIGAL-SANTILLAN, E., BAUTISTA, M., ESQUIVEL-SOTO, J., MORALES-GONZALEZ, A., ESQUIVEL-CHIRINO, C., DURANTE-MONTIEL, I., SANCHEZ-RIVERA, G., VALADEZ-VEGA, C. & MORALES-GONZALEZ, J. A. 2011. Inflammation, oxidative stress, and obesity. *Int J Mol Sci,* 12, 3117-32.

FLEMING, I. & BUSSE, R. 2003. Molecular mechanisms involved in the regulation of the endothelial nitric oxide synthase. *Am J Physiol Regul Integr Comp Physiol,* 284, R1-12.

FURUKAWA, S., FUJITA, T., SHIMABUKURO, M., IWAKI, M., YAMADA, Y., NAKAJIMA, Y., NAKAYAMA, O., MAKISHIMA, M., MATSUDA, M. & SHIMOMURA, I. 2004. Increased oxidative stress in obesity and its impact on metabolic syndrome. *J Clin Invest,* 114, 1752-61.

GIORGIO, M., MIGLIACCIO, E., ORSINI, F., PAOLUCCI, D., MORONI, M., CONTURSI, C., PELLICCIA, G., LUZI, L., MINUCCI, S., MARCACCIO, M., PINTON, P., RIZZUTO, R., BERNARDI, P., PAOLUCCI, F. & PELICCI, P. G. 2005. Electron transfer between cytochrome c and p66Shc generates reactive oxygen species that trigger mitochondrial apoptosis. *Cell,* 122, 221-33.

HARDY, L. L., WICK, D. A. & WEBB, J. R. 2008. Conversion of tyrosine to the inflammation-associated analog 3'-nitrotyrosine at either TCR- or MHC-contact positions can profoundly affect recognition of the MHC class I-restricted epitope of lymphocytic choriomeningitis virus glycoprotein 33 by CD8 T cells. *J Immunol,* 180, 5956-62.

HEALY, G. N., WIJNDAELE, K., DUNSTAN, D. W., SHAW, J. E., SALMON, J., ZIMMET, P. Z. & OWEN, N. 2008. Objectively measured sedentary time, physical activity, and metabolic risk: the Australian Diabetes, Obesity and Lifestyle Study (AusDiab). *Diabetes Care,* 31, 369-71.

HORI, Y. S., KUNO, A., HOSODA, R. & HORIO, Y. 2013. Regulation of FOXOs and p53 by SIRT1 modulators under oxidative stress. *PLoS One,* 8, e73875.

HORI, Y. S., KUNO, A., HOSODA, R., TANNO, M., MIURA, T., SHIMAMOTO, K. & HORIO, Y. 2011. Resveratrol ameliorates muscular pathology in the dystrophic mdx mouse, a model for Duchenne muscular dystrophy. *J Pharmacol Exp Ther,* 338, 784-94.

HOTAMISLIGIL, G. S. 2006. Inflammation and metabolic disorders. *Nature,* 444, 860-7.

HWANG, J. W., YAO, H., CAITO, S., SUNDAR, I. K. & RAHMAN, I. 2013. Redox regulation of SIRT1 in inflammation and cellular senescence. *Free Radic Biol Med,* 61, 95-110.

ICHIDA, K., AMAYA, Y., OKAMOTO, K. & NISHINO, T. 2012. Mutations associated with functional disorder of xanthine oxidoreductase and hereditary xanthinuria in humans. *Int J Mol Sci,* 13, 15475-95.

JAESCHKE, H., GORES, G. J., CEDERBAUM, A. I., HINSON, J. A., PESSAYRE, D. & LEMASTERS, J. J. 2002. Mechanisms of hepatotoxicity. *Toxicol Sci,* 65, 166-76.

JIANG, F., LIM, H. K., MORRIS, M. J., PRIOR, L., VELKOSKA, E., WU, X. & DUSTING, G. J. 2011. Systemic upregulation of NADPH oxidase in diet-induced obesity in rats. *Redox Rep,* 16, 223-9.

JIANG, J., SHI, Y., SHAN, Z., YANG, L., WANG, X. & SHI, L. 2012. Bioaccumulation, oxidative stress and HSP70 expression in Cyprinus carpio L. exposed to microcystin-LR under laboratory conditions. *Comp Biochem Physiol C Toxicol Pharmacol,* 155, 483-90.

KATAKAM, P. V., TULBERT, C. D., SNIPES, J. A., ERDÖS, B., MILLER, A. W. & BUSIJA, D. W. 2005. Impaired insulin-induced vasodilation in small coronary arteries of Zucker obese rats is mediated by reactive oxygen species. *American Journal of Physiology-Heart and Circulatory Physiology,* 288, H854-H860.

KAWASHIMA, S. & YOKOYAMA, M. 2004a. Dysfunction of endothelial nitric oxide synthase and atherosclerosis. *Arteriosclerosis, thrombosis, and vascular biology,* 24, 998-1005.

KAWASHIMA, S. & YOKOYAMA, M. 2004b. Dysfunction of endothelial nitric oxide synthase and atherosclerosis. *Arterioscler Thromb Vasc Biol,* 24, 998-1005.

KHANDAY, F. A., SANTHANAM, L., KASUNO, K., YAMAMORI, T., NAQVI, A., DERICCO, J., BUGAYENKO, A., MATTAGAJASINGH, I., DISANZA, A., SCITA, G. & IRANI, K. 2006. Sos-mediated activation of rac1 by p66shc. *J Cell Biol,* 172, 817-22.

KUBOKI, K., JIANG, Z. Y., TAKAHARA, N., HA, S. W., IGARASHI, M., YAMAUCHI, T., FEENER, E. P., HERBERT, T. P., RHODES, C. J. & KING, G. L. 2000. Regulation of endothelial constitutive nitric oxide synthase gene expression in endothelial cells and in vivo : a specific vascular action of insulin. *Circulation,* 101, 676-81.

KUMAR, S., SUN, X., WISEMAN, D. A., TIAN, J., UMAPATHY, N. S., VERIN, A. D. & BLACK, S. M. 2009. Hydrogen peroxide decreases endothelial nitric oxide synthase promoter activity through the inhibition of Sp1 activity. *DNA Cell Biol,* 28, 119-29.

LASSEGUE, B. & GRIENDLING, K. K. 2010. NADPH oxidases: functions and pathologies in the vasculature. *Arterioscler Thromb Vasc Biol,* 30, 653-61.

LI, J. M., FAN, L. M., CHRISTIE, M. R. & SHAH, A. M. 2005. Acute tumor necrosis factor alpha signaling via NADPH oxidase in microvascular endothelial cells: role of p47phox phosphorylation and binding to TRAF4. *Mol Cell Biol,* 25, 2320-30.

LI, X., ZHANG, S., BLANDER, G., TSE, J. G., KRIEGER, M. & GUARENTE, L. 2007. SIRT1 deacetylates and positively regulates the nuclear receptor LXR. *Mol Cell,* 28, 91-106.

LYNCH, S. M., FREI, B., MORROW, J. D., ROBERTS, L. J., 2ND, XU, A., JACKSON, T., REYNA, R., KLEVAY, L. M., VITA, J. A. & KEANEY, J. F., JR. 1997. Vascular superoxide dismutase deficiency impairs endothelial vasodilator function through direct inactivation of nitric oxide and increased lipid peroxidation. *Arterioscler Thromb Vasc Biol,* 17, 2975-81.

MALHOTRA, A., VASHISTHA, H., YADAV, V. S., DUBE, M. G., KALRA, S. P., ABDELLATIF, M. & MEGGS, L. G. 2009. Inhibition of p66ShcA redox activity in cardiac muscle cells attenuates hyperglycemia-induced oxidative stress and apoptosis. *Am J Physiol Heart Circ Physiol,* 296, H380-8.

MANSON, J. E., SKERRETT, P. J., GREENLAND, P. & VANITALLIE, T. B. 2004. The escalating pandemics of obesity and sedentary lifestyle: a call to action for clinicians. *Archives of Internal Medicine,* 164, 249-258.

MATTAGAJASINGH, I., KIM, C. S., NAQVI, A., YAMAMORI, T., HOFFMAN, T. A., JUNG, S. B., DERICCO, J., KASUNO, K. & IRANI, K. 2007. SIRT1 promotes endothelium-dependent vascular relaxation by activating endothelial nitric oxide synthase. *Proc Natl Acad Sci U S A,* 104, 14855-60.

MILLER, A. A., DRUMMOND, G. R., MAST, A. E., SCHMIDT, H. H. & SOBEY, C. G. 2007. Effect of gender on NADPH-oxidase activity, expression, and function in the cerebral circulation: role of estrogen. *Stroke,* 38, 2142-9.

MILLER, A. A., DRUMMOND, G. R., SCHMIDT, H. H. & SOBEY, C. G. 2005. NADPH oxidase activity and function are profoundly greater in cerebral versus systemic arteries. *Circ Res,* 97, 1055-62.

MONTERO, J., DUTTA, C., VAN BODEGOM, D., WEINSTOCK, D. & LETAI, A. 2013. p53 regulates a non-apoptotic death induced by ROS. *Cell Death Differ,* 20, 1465-74.
NEMOTO, S. & FINKEL, T. 2002. Redox regulation of forkhead proteins through a p66shc-dependent signaling pathway. *Science,* 295, 2450-2.

OLMOS, Y., SANCHEZ-GOMEZ, F. J., WILD, B., GARCIA-QUINTANS, N., CABEZUDO, S., LAMAS, S. & MONSALVE, M. 2013. SirT1 regulation of antioxidant genes is dependent on the formation of a FoxO3a/PGC-1alpha complex. *Antioxid Redox Signal,* 19, 1507-21.

OLMOS, Y., VALLE, I., BORNIQUEL, S., TIERREZ, A., SORIA, E., LAMAS, S. & MONSALVE, M. 2009. Mutual dependence of Foxo3a and PGC-1alpha in the induction of oxidative stress genes. *J Biol Chem,* 284, 14476-84.

OTA, H., AKISHITA, M., ETO, M., IIJIMA, K., KANEKI, M. & OUCHI, Y. 2007. Sirt1 modulates premature senescence-like phenotype in human endothelial cells. *J Mol Cell Cardiol,* 43, 571-9.

OTA, H., ETO, M., KANO, M. R., KAHYO, T., SETOU, M., OGAWA, S., IIJIMA, K., AKISHITA, M. & OUCHI, Y. 2010. Induction of endothelial nitric oxide synthase, SIRT1, and catalase by statins inhibits endothelial senescence through the Akt pathway. *Arterioscler Thromb Vasc Biol,* 30, 2205-11.

PANENI, F., MOCHARLA, P., AKHMEDOV, A., COSTANTINO, S., OSTO, E., VOLPE, M., LUSCHER, T. F. & COSENTINO, F. 2012. Gene silencing of the mitochondrial adaptor p66(Shc) suppresses vascular hyperglycemic memory in diabetes. *Circ Res,* 111, 278-89.

PEETERS, A. V., BECKERS, S., VERRIJKEN, A., MERTENS, I., ROEVENS, P., PEETERS, P. J., VAN HUL, W. & VAN GAAL, L. F. 2008. Association of SIRT1 gene variation with visceral obesity. *Hum Genet,* 124, 431-6.

PFLUGER, P. T., HERRANZ, D., VELASCO-MIGUEL, S., SERRANO, M. & TSCHOP, M. H. 2008. Sirt1 protects against high-fat diet-induced metabolic damage. *Proc Natl Acad Sci U S A,* 105, 9793-8.

PICARD, F., GEHIN, M., ANNICOTTE, J., ROCCHI, S., CHAMPY, M. F., O'MALLEY, B. W., CHAMBON, P. & AUWERX, J. 2002. SRC-1 and TIF2 control energy balance between white and brown adipose tissues. *Cell,* 111, 931-41.

PUIGSERVER, P., WU, Z., PARK, C. W., GRAVES, R., WRIGHT, M. & SPIEGELMAN, B. M. 1998. A cold-inducible coactivator of nuclear receptors linked to adaptive thermogenesis. *Cell,* 92, 829-39.

ROOS, C. M., HAGLER, M., ZHANG, B., OEHLER, E. A., ARGHAMI, A. & MILLER, J. D. 2013. Transcriptional and phenotypic changes in aorta and aortic valve with aging and MnSOD deficiency in mice. *Am J Physiol Heart Circ Physiol,* 305, H1428-39.

SCHACHINGER, V., BRITTEN, M. B. & ZEIHER, A. M. 2000. Prognostic impact of coronary vasodilator dysfunction on adverse long-term outcome of coronary heart disease. *Circulation,* 101, 1899-906.

SCHRAUWEN, P., HOEKS, J. & HESSELINK, M. K. 2006a. Putative function and physiological relevance of the mitochondrial uncoupling protein-3: involvement in fatty acid metabolism? *Prog Lipid Res,* 45, 17-41.

SCHRAUWEN, P., HOEKS, J. & HESSELINK, M. K. C. 2006b. Putative function and physiological relevance of the mitochondrial uncoupling protein-3: Involvement in fatty acid metabolism? *Progress in Lipid Research,* 45, 17-41.

SEGAL, A. W. & JONES, O. T. 1978. Novel cytochrome b system in phagocytic vacuoles of human granulocytes. *Nature,* 276, 515-7.

SELLAYAH, D., SEK, K., ANTHONY, F. W., HANSON, M. A. & CAGAMPANG, F. R. 2008. Sensitivity of housekeeping genes in the hypothalamus to mismatch in diets between pre- and postnatal periods in mice. *Neurosci Lett,* 447, 54-7.

STATISTICS, A. B. O. 2012. Australian Health Survey: First Results, 2011-12

SUN, Y., ST CLAIR, D. K., XU, Y., CROOKS, P. A. & ST CLAIR, W. H. 2010. A NADPH oxidase-dependent redox signaling pathway mediates the selective radiosensitization effect of parthenolide in prostate cancer cells. *Cancer Res,* 70, 2880-90.

TAJBAKHSH, N. & SOKOYA, E. M. 2012. Regulation of cerebral vascular function by sirtuin 1. *Microcirculation,* 19, 336-42.

TESAURO, M., SCHINZARI, F., IANTORNO, M., RIZZA, S., MELINA, D., LAURO, D. & CARDILLO, C. 2005. Ghrelin improves endothelial function in patients with metabolic syndrome. *Circulation,* 112, 2986-92.

TRACHOOTHAM, D., LU, W., OGASAWARA, M. A., NILSA, R. D. & HUANG, P. 2008. Redox regulation of cell survival. *Antioxid Redox Signal,* 10, 1343-74.

VALLE, I., ALVAREZ-BARRIENTOS, A., ARZA, E., LAMAS, S. & MONSALVE, M. 2005. PGC-1alpha regulates the mitochondrial antioxidant defense system in vascular endothelial cells. *Cardiovasc Res,* 66, 562-73.

VAZIRI, H., DESSAIN, S. K., NG EATON, E., IMAI, S. I., FRYE, R. A., PANDITA, T. K., GUARENTE, L. & WEINBERG, R. A. 2001. hSIR2(SIRT1) functions as an NAD-dependent p53 deacetylase. *Cell,* 107, 149-59.

WANG, B., SHRAVAH, J., LUO, H., RAEDSCHELDERS, K., CHEN, D. D. & ANSLEY, D. M. 2009. Propofol protects against hydrogen peroxide-induced injury in cardiac H9c2 cells via Akt activation and Bcl-2 up-regulation. *Biochem Biophys Res Commun,* 389, 105-11.

WANG, Y., BEYDOUN, M. A., LIANG, L., CABALLERO, B. & KUMANYIKA, S. K. 2008. Will all Americans become overweight or obese? estimating the progression and cost of the US obesity epidemic. *Obesity (Silver Spring),* 16, 2323-30.

WEIGLE, D. S., SELFRIDGE, L. E., SCHWARTZ, M. W., SEELEY, R. J., CUMMINGS, D. E., HAVEL, P. J., KUIJPER, J. L. & BELTRANDELRIO, H. 1998. Elevated free fatty acids induce uncoupling protein 3 expression in muscle: a potential explanation for the effect of fasting. *Diabetes,* 47, 298-302.

WEISIGER, R. A. & FRIDOVICH, I. 1973. Superoxide dismutase. Organelle specificity. *J Biol Chem,* 248, 3582-92.

WHO 2000. *Obesity: preventing and managing the global epidemic*, World Health Organization.

World Heart Federation 2014. *Cardiovascular disease risk factors*,Geneva, viewed 3 April 2014,<http://www.world-heart-federation.org/cardiovascular-health/cardiovascular-disease-risk-factors>.

WU, H. & BALLANTYNE, C. M. 2014. Inflammation versus Host Defense in Obesity. *Cell Metab,* 20, 708-9.

ZARZUELO, M. J., LOPEZ-SEPULVEDA, R., SANCHEZ, M., ROMERO, M., GOMEZ-GUZMAN, M., UNGVARY, Z., PEREZ-VIZCAINO, F., JIMENEZ, R. & DUARTE, J. 2013. SIRT1 inhibits NADPH oxidase activation and protects endothelial function in the rat aorta: implications for vascular aging. *Biochem Pharmacol,* 85, 1288-96.

ZHANG, Q. J., WANG, Z., CHEN, H. Z., ZHOU, S., ZHENG, W., LIU, G., WEI, Y. S., CAI, H., LIU, D. P. & LIANG, C. C. 2008. Endothelium-specific overexpression of class III deacetylase SIRT1 decreases atherosclerosis in apolipoprotein E-deficient mice. *Cardiovasc Res,* 80, 191-9.

ZHOU, S., CHEN, H. Z., WAN, Y. Z., ZHANG, Q. J., WEI, Y. S., HUANG, S., LIU, J. J., LU, Y. B., ZHANG, Z. Q., YANG, R. F., ZHANG, R., CAI, H., LIU, D. P. & LIANG, C. C. 2011. Repression of P66Shc expression by SIRT1 contributes to the prevention of hyperglycemia-induced endothelial dysfunction. *Circ Res,* 109, 639-48.

ZILLIKENS, M. C., VAN MEURS, J. B., RIVADENEIRA, F., AMIN, N., HOFMAN, A., OOSTRA, B. A., SIJBRANDS, E. J., WITTEMAN, J. C., POLS, H. A., VAN DUIJN, C. M. & UITTERLINDEN, A. G. 2009. SIRT1 genetic variation is related to BMI and risk of obesity. *Diabetes,* 58, 2828-34.

APPENDICES

Appendix 1: RNA Concentrations Measured by Using Thermo Scientific NanoDrop 2000 Spectrophotometer.

RNA Sample	Concentration (µg/mL)	A260 (10 mm path)	A280 (10 mm path)	260/280	260/230
SRT 2-4 HF WT	111.20	2.77	1.82	1.52	0.25
SRT 4-4 NC WT	59.10	1.48	1.01	1.47	0.24
SRT 4-2 HF TG	116.40	2.91	1.92	1.52	0.31
SRT 4-1 NC TG	111.75	2.79	1.86	1.51	0.29
SRT 5-1 HF WT	48.75	1.22	0.81	1.50	0.25
SRT 10-1 NC WT	79.10	1.98	1.34	1.48	0.25
SRT 18-2 HF TG	90.80	2.27	1.54	1.48	0.22
SRT 18-1 HF WT	244.65	6.12	3.65	1.68	0.37
SRT 10-2 NC WT	261.45	6.54	3.89	1.68	0.38
SRT 18-3 HF TG	176.30	4.41	2.78	1.59	0.27
SRT 18-4 HF WT	78.00	1.95	1.31	1.49	0.22
SRT 15-1 NC WT	74.30	1.86	1.28	1.46	0.17
SRT 19-2 HF TG	85.40	2.14	1.39	1.54	0.23
SRT 16-1 NC TG	90.00	2.25	1.51	1.49	0.25
SRT 21-1 NC TG	94.75	2.37	1.58	1.50	0.25
SRT 17-4 NC TG	94.75	2.37	1.64	1.45	0.23
SRT 19-1 HF WT	97.40	2.44	1.56	1.56	0.26
SRT 19-3 HF WT	80.00	2.00	1.30	1.55	0.29
SRT 19-4 HF TG	90.15	2.25	1.45	1.56	0.29
SRT 17-2 NC TG	84.75	2.12	1.37	1.55	0.23
SRT 20-3 TG HF	54.55	1.36	0.92	1.48	0.23
SRT 15-2 NC TG	45.15	1.13	0.80	1.42	0.19

Appendix 2: Bioanalyser Results and RIN Values
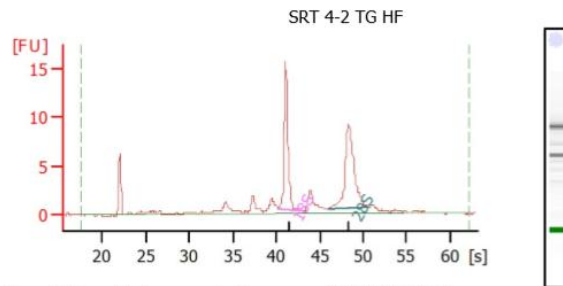
SRT 4-2 TG HF

Overall Results for sample 9 :   **SRT 4-2 TG HF**

RNA Area:	78.1
RNA Concentration:	261 pg/µl
rRNA Ratio [28s / 18s]:	1.2
RNA Integrity Number (RIN):	8.5 (B.02.08)
Result Flagging Color:	
Result Flagging Label:	RIN: 8.50

Fragment table for sample 9 :   **SRT 4-2 TG HF**

Name	Start Time [s]	End Time [s]	Area	% of total Area
18S	40.17	42.96	19.0	24.3
28S	45.94	50.67	22.0	28.1
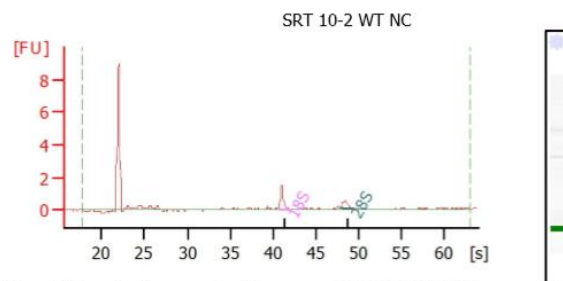
SRT 10-2 WT NC

Overall Results for sample 11 :   **SRT 10-2 WT NC**

RNA Area:	6.0
RNA Concentration:	20 pg/µl
rRNA Ratio [28s / 18s]:	0.5
RNA Integrity Number (RIN):	7.8 (B.02.08)
Result Flagging Color:	
Result Flagging Label:	RIN: 7.80

Fragment table for sample 11 :   **SRT 10-2 WT NC**

Name	Start Time [s]	End Time [s]	Area	% of total Area
18S	40.58	41.99	1.5	25.5
28S	47.74	49.75	0.7	12.4
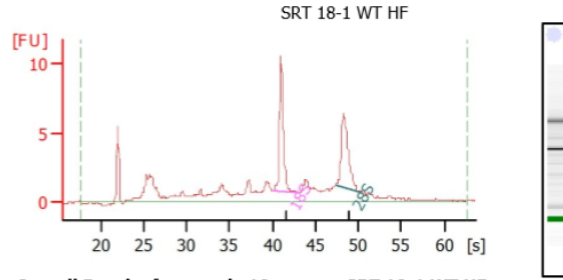
SRT 18-1 WT HF

Overall Results for sample 10 :   SRT 18-1 WT HF

RNA Area:	85.5
RNA Concentration:	286 pg/µl
rRNA Ratio [28s / 18s]:	0.9
RNA Integrity Number (RIN):	7.1 (B.02.08)
Result Flagging Color:	
Result Flagging Label:	RIN: 7.10

Fragment table for sample 10 :   SRT 18-1 WT HF

Name	Start Time [s]	End Time [s]	Area	% of total Area
18S	40.05	43.09	12.3	14.4
28S	47.41	50.50	10.6	12.4
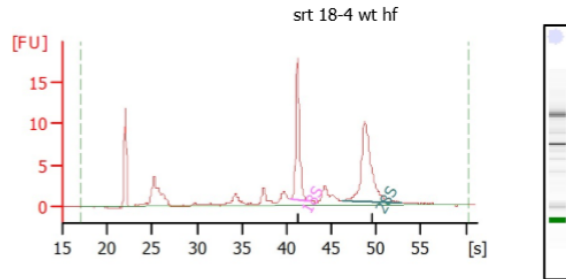
srt 18-4 wt hf

Overall Results for sample 2 :   srt 18-4 wt hf

RNA Area:	95.2
RNA Concentration:	166 pg/µl
rRNA Ratio [28s / 18s]:	1.3
RNA Integrity Number (RIN):	8.6 (B.02.08)
Result Flagging Color:	
Result Flagging Label:	RIN: 8.60

Fragment table for sample 2 :   srt 18-4 wt hf

Name	Start Time [s]	End Time [s]	Area	% of total Area
18S	40.37	42.34	19.4	20.4
28S	46.23	52.79	25.8	27.1

srt 19-2 tg hf
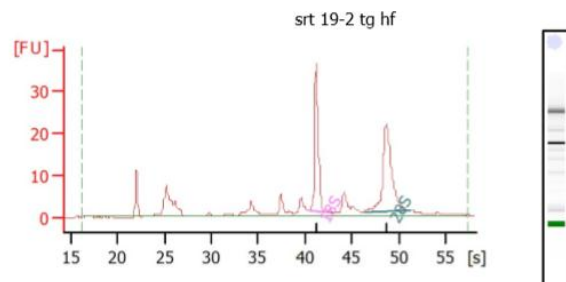
Overall Results for sample 5 :   srt 19-2 tg hf

RNA Area:	183.3
RNA Concentration:	319 pg/µl
rRNA Ratio [28s / 18s]:	1.2
RNA Integrity Number (RIN):	8.6 (B.02.08)
Result Flagging Color:	
Result Flagging Label:	RIN: 8.60

Fragment table for sample 5 :   srt 19-2 tg hf

Name	Start Time [s]	End Time [s]	Area	% of total Area
18S	40.34	42.21	38.6	21.1
28S	46.29	51.24	47.4	25.9
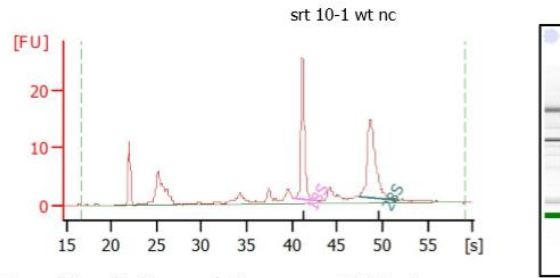
srt 10-1 wt nc

Overall Results for sample 3 :   <u>srt 10-1 wt nc</u>

RNA Area:	129.4
RNA Concentration:	225 pg/µl
rRNA Ratio [28s / 18s]:	1.1
RNA Integrity Number (RIN):	8.5 (B.02.08)
Result Flagging Color:	
Result Flagging Label:	RIN: 8.50

Fragment table for sample 3 :   <u>srt 10-1 wt nc</u>

Name	Start Time [s]	End Time [s]	Area	% of total Area
18S	40.27	42.20	27.6	21.3
28S	47.39	51.72	29.9	23.1

srt 16-1 tg nc
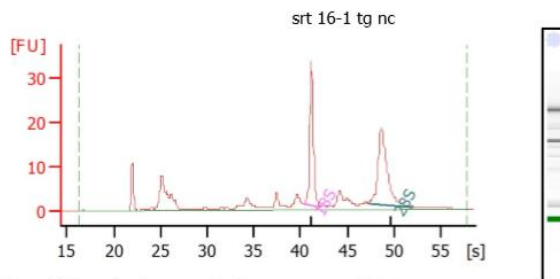
Overall Results for sample 7 :   <u>srt 16-1 tg nc</u>

RNA Area:	166.1
RNA Concentration:	289 pg/µl
rRNA Ratio [28s / 18s]:	1.1
RNA Integrity Number (RIN):	8.5 (B.02.08)
Result Flagging Color:	
Result Flagging Label:	RIN: 8.50

Fragment table for sample 7 :   <u>srt 16-1 tg nc</u>

Name	Start Time [s]	End Time [s]	Area	% of total Area
18S	40.31	42.16	35.6	21.4
28S	47.23	52.05	39.9	24.0

srt 17-4 tg nc
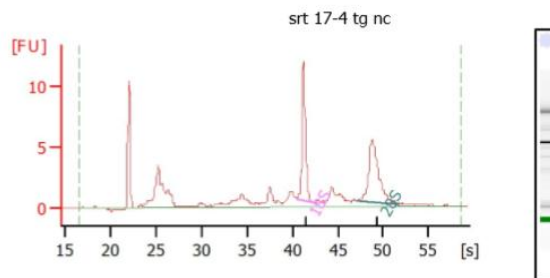
Overall Results for sample 8 :   <u>srt 17-4 tg nc</u>

RNA Area:	71.2
RNA Concentration:	124 pg/µl
rRNA Ratio [28s / 18s]:	1.1
RNA Integrity Number (RIN):	7.9 (B.02.08)
Result Flagging Color:	
Result Flagging Label:	RIN: 7.90

Fragment table for sample 8 :   <u>srt 17-4 tg nc</u>

Name	Start Time [s]	End Time [s]	Area	% of total Area
18S	40.52	42.39	12.5	17.6
28S	47.14	51.73	13.5	18.9

srt 11-1 tg nc
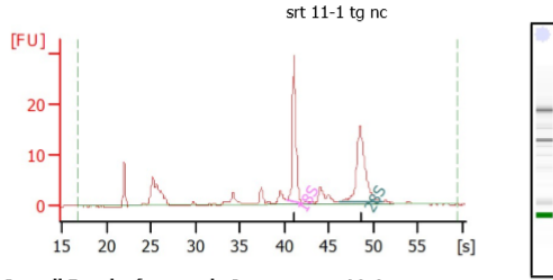
Overall Results for sample 9 :   <u>srt 11-1 tg nc</u>

RNA Area:	133.8
RNA Concentration:	233 pg/µl
rRNA Ratio [28s / 18s]:	1.1
RNA Integrity Number (RIN):	8.7 (B.02.08)
Result Flagging Color:	
Result Flagging Label:	RIN: 8.70

Fragment table for sample 9 :   <u>srt 11-1 tg nc</u>

Name	Start Time [s]	End Time [s]	Area	% of total Area
18S	40.25	42.10	31.4	23.5
28S	46.20	51.16	33.7	25.2

srt 4-1 tg nc
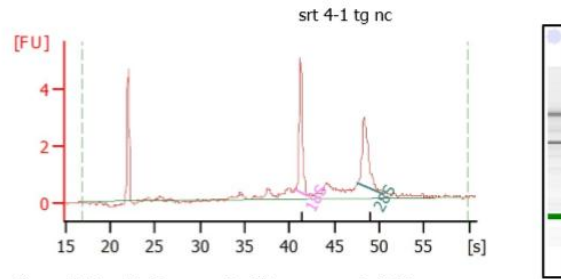
Overall Results for sample 10 :   <u>srt 4-1 tg nc</u>

RNA Area:	21.2
RNA Concentration:	37 pg/µl
rRNA Ratio [28s / 18s]:	0.8
RNA Integrity Number (RIN):	7.8 (B.02.08)
Result Flagging Color:	
Result Flagging Label:	RIN: 7.80

Fragment table for sample 10 :   <u>srt 4-1 tg nc</u>

Name	Start Time [s]	End Time [s]	Area	% of total Area
18S	40.70	42.00	4.7	22.4
28S	47.60	50.42	4.0	19.0
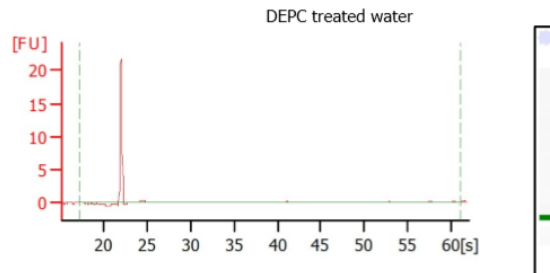
DEPC treated water

Overall Results for sample 11 :   <u>DEPC treated water</u>

RNA Area:	6.3
RNA Concentration:	11 pg/µl
rRNA Ratio [28s / 18s]:	0.0
RNA Integrity Number (RIN):	1 (B.02.08)
Result Flagging Color:	
Result Flagging Label:	RIN:1

Appendix 3: Protein Extraction Buffer Components

Final Concentration	Supplier	MW	Concentration (g/L)	Weight for 100ml
50mM Tris, pH 8.0	Sigma;T6791	121.1	6.055 g/L	0.6055 g
2% w/v SDS	BioRad; 161-0416 10% w/v solution			20ml
Milli-Q H$_2$O				make up to 100ml
On the day of use add the following to a 10ml aliquot of above				
5mM DTT	BioRad; 161-0611	154.3		0.007715g
Add 1 Protease Inhibitor Tablet with EDTA to 10ml	Roche; 11836153001			

Notes:
✱ Highlighted cell is a detergent. pH to 8.0 before adding detergent.
* Store 10ml aliquots at -20˚C.
* Note that SDS comes about of solution when it cools.

Samples: Two mouse carotid arteries snap frozen in 30ul PEB without detergent (from Tony Donato's lab).

Appendix 4:   **Composition of 4X Sample Buffer**

Table. 4X Treatment (Sample) Buffer (10mL)

4X Stack Gel Buffer (0.5 M Tris-HCL pH 6.8)	5.0 mL
Glyserol	4.0 mL
SDS	0.8 g
Bromophenol Blue	0.004 g

1.   Note: Sometimes the BP blue will need to be omitted, such as when performing an EZQ assay on the sample.
2.   Mix together everything in a 10 mL final volume.
3.   Make 1 mL aliquots and freeze at -20°C.

***Add DTT fresh before running the gel (4mg in 100 µl Sample Buffer).